Review

Chiral Effective Model of Cold and Dense Two-Color QCD: The Linear Sigma Model Approach

Daiki Suenaga

Kobayashi-Maskawa Institute for the Origin of Particles and the Universe, Nagoya University, Nagoya 464-8602, Japan; suenaga.daiki.j1@f.mail.nagoya-u.ac.jp

Abstract: This review is devoted to summarizing recent developments of the linear sigma model (LSM) in cold and dense two-color QCD (QC$_2$D), in which lattice simulations are straightforwardly applicable thanks to the disappearance of the sign problem. In QC$_2$D, both theoretical and numerical studies derive the presence of the so-called baryon superfluid phase at a sufficiently large chemical potential (μ_q), where diquark condensates govern the ground state. The hadron mass spectrum simulated in this phase shows that the mass of an iso-singlet ($I = 0$) and 0^- state is remarkably reduced, but such a mode cannot be described by the chiral perturbation theory. Motivated by this fact, I have invented a LSM constructed upon the linear representation of chiral symmetry, more precisely Pauli–Gürsey symmetry. It is shown that my LSM successfully reproduces the low-lying hadron mass spectrum in a broad range of μ_q simulated on the lattice. As applications of the LSM, topological susceptibility and sound velocity in cold and dense QC$_2$D are evaluated to compare with the lattice results. Additionally, the generalized Gell–Mann–Oakes–Renner relation and hardon mass spectrum in the presence of a diquark source are analyzed. I also introduce an extended version of the LSM incorporating spin-1 hadrons.

Keywords: two-color QCD; linear sigma model; chiral effective model; lattice QCD simulation; cold and dense QCD; baryon superfluid phase

1. Introduction

In recent years, the elucidation of quantum chromodynamics (QCD) in cold and dense systems has gathered much attention, motivated by the progress of neutron star observations [1]. In these dense system, quarks confined inside hadrons begin to overlap as the density increases, and finally, quark degrees of freedom govern the matter. Due to the complexity stemming from the strong coupling and nonperturbative nature of QCD, however, it is not easy to unveil this transition in detail.

One of the most powerful tools to shed light on the QCD problem is the first-principles *lattice QCD simulation*. However, lattice simulations with a chemical potential at a lower temperature are not straightforward due to the so-called *sign problem* of the Monte Carlo computation [2,3]. Additionally, considering the current difficulty of accelerator experiments, cold and dense QCD can be regarded as a frontier of quark–hadron physics.

The sign problem of lattice simulations occurs when the path integral yields complex values. Hence, when we focus on two-color QCD (QC$_2$D) where the gluodynamics is governed by the $SU(2)_c$ gauge theory possessing pseudoreality, the troublesome sign problem disappears. This advantage enables us to apply the lattice simulation straightforwardly even in a cold and dense system. Indeed, thus far, lattice simulations in QC$_2$D with a baryon-number (or a quark-number) chemical potential have been conducted by several

groups to explore the phase diagram with order parameters, hadron masses, thermodynamic properties, gluondynamics, transport coefficients, and so on [4–34].

In the QC$_2$D world, the pseudoreal nature of the $SU(2)_c$ gauge theory allows us to treat a quark and an antiquark belonging to **2** and **2*** representations on an equal footing. As a result, at a hadronic level, for instance, certain mesons and diquarks share the same properties. In terms of the flavor representation, this is reflected by the enlargement of chiral symmetry; $SU(N_f)_L \times SU(N_f)_R$ chiral symmetry is extended to the so-called *Pauli–Gürsey* $SU(2N_f)$ *symmetry* in QC$_2$D [35,36].

Since (anti)diquarks are bosonic in QC$_2$D, obeying Bose–Einstein statistics similarly to mesons, they start to exhibit Bose–Einstein condensations (BECs) at an adequately large chemical potential μ_q. This condensed phase is referred to simply as the *diquark condensed phase*, or the *baryon superfluid phase* to stress the $U(1)$ baryon-number violation with no breakdown of color symmetry. Meanwhile, the calm phase connected to the vacuum (zero temperature and zero chemical potential) is called the *hadronic phase*.

A schematic picture of a QC$_2$D phase diagram is depicted in Figure 1. In this figure, the Bardeen–Cooper–Schrieffer (BCS) regime in the baryon superfluid phase is defined by which the quark density n_q is consistent with the Stefan–Boltzmann-limit value of free quarks n_q^{SB}: $n_q/n_q^{SB} \approx 1$. Accordingly, in the BEC regime, $n_q/n_q^{SB} < 1$.
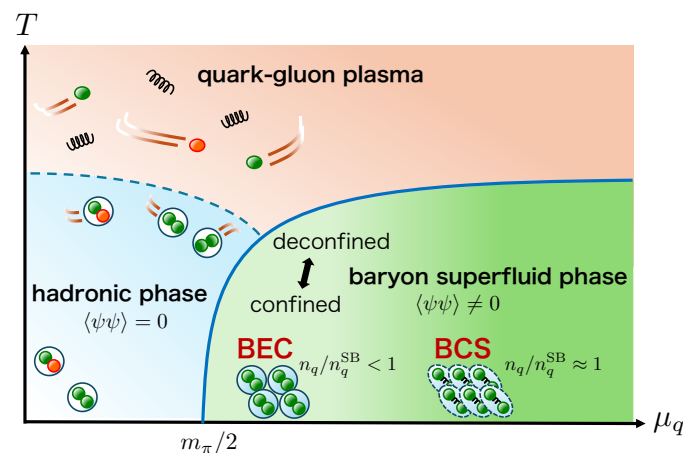
Figure 1. A schematic phase diagram of QC$_2$D.

In order to gain qualitative and predictive insights into the *numerical experiments* of cold and dense QC$_2$D performed on lattice, it is inevitable to translate the numerical results in terms of appropriate effective degrees of freedom. In the low-energy regime of QC$_2$D where the system is governed by highly nonperturbative dynamics, such excitations are brought about by light hadrons. Hence, hadron effective models can be regarded as useful tools there. The lattice results predict sufficiently suppressed Polyakov loops even in the dense regime [22,34], indicating that hadronic and quark matters are connected by crossover. Therefore, hadron effective models would be able to explore the deeper regime of dense QC$_2$D.

The spirit of hadron effective models is expressed by the following matching equality [37,38],

$$Z_{QC_2D} = Z_{\text{eff. model}} ,\qquad (1)$$

where the left-hand side (LHS) and right-hand side (RHS) stand for the generating functionals of underlying QC$_2$D and of an effective model, respectively. That is, (maybe concise)

quantum theory developed in hadron effective models must match that of the nonperturbative QC_2D model at low energy. More practically, we make use of

$$\Gamma_{QC_2D} = \Gamma_{eff.\ model} \qquad (2)$$

as the matching condition, with the corresponding effective action $\Gamma = -i\ln Z$. This Γ can be regarded as an action incorporating quantum corrections, so that symmetry properties inhabiting QC_2D at a quantum level must be mimicked by the effective model properties. Those matching properties are the essential points when adopting hadron effective models.

The (approximate) Pauli–Gürsey $SU(2N_f)$ symmetry is spontaneously broken due to the emergence of chiral condensates $\langle\bar{\psi}\psi\rangle$ in the vacuum, the breaking pattern of which is $SU(2N_f) \to Sp(2N_f)$ for identical quark masses [39,40]. Accordingly, the Nambu–Goldstone (NG) bosons dominate over the low-energy dynamics of QC_2D. Due to the equal treatment of certain mesons and diquarks, those NG bosons are played by $N_f^2 - 1$ pions and $N_f^2 - N_f$ flavor-singlet scalar (anti)diquarks.

When describing those NG boson dynamics, the chiral perturbation theory (ChPT) framework is useful thanks to its systematic low-energy expansion; it was developed in Refs. [39,40]. Indeed, this effective model successfully reproduces, e.g., hadron masses [11,41] and sound velocity [30,34] measured on the lattice for $N_f = 2$, in the vicinity of the phase transition to the baryon superfluid phase. However, since the ChPT is based on the low-energy expansion for only the NG bosons where other excitations are integrated out [42,43], it is unclear whether the ChPT framework still works at larger μ_q. Moreover, the recent lattice results in Ref. [41] indicate that the next-lightest excitation in the superfluid phase is an iso-singlet mode carrying a negative parity ($I = 0, 0^-$), which cannot be handled by the ChPT, as depicted in Figure 2. These facts require us to extend the ChPT to describe other hadrons including the $I = 0, 0^-$ mode for which the low-energy spectrum of dense QC_2D is appropriately delineated.
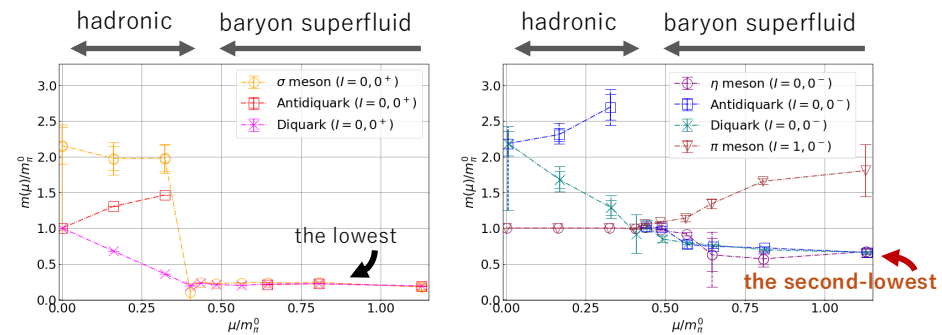
Figure 2. μ_q dependences of the spin-0 hadron masses at a low temperature, which were computed in Ref. [41]. The second-lowest state ($I = 0, 0^-$) in the superfluid phase cannot be described in the ChPT framework.

Motivated by this fact, I invented a linear sigma model (LSM) as an extension of the ChPT based on the linear representation of the Pauli–Gürsey symmetry for $N_f = 2$ [44]. This effective model allows us to describe not only the NG bosons such as the pions and 0^+ diquarks but also the scalar mesons and 0^- diquarks collectively, although the systematics is rather obscure. The latter hadrons are referred to as the *parity partners* or *chiral partners* to the NG bosons, which are predicted to degenerate with the NG bosons at the chiral restoration point. Additionally, the linear representation of the LSM implies its validity at a rather high μ_q, where the nonlinearly realized ChPT framework cannot affect it, since chiral symmetry is restored at a sufficiently large μ_q.

In addition to the ChPT and LSM approaches, other effective models containing quark–gluon degrees of freedom such as the Nambu–Jona–Lasinio (NJL) and massive gluon model were employed to theoretically examine cold and dense QC_2D properties [39,40,44–74].

In this review, I summarize the main points of Refs. [44,70–72] achieved within the LSM framework. Since effective models such as the LSM must obey QC_2D-inspired symmetry properties due to the matching condition of Equation (1) or Equation (2), first in Section 2, I explain the Ward–Takahashi identities (WTIs) related to the spontaneous breakdown of the Pauli–Gürsey symmetry from the underlying QC_2D theory. Next, in Section 3, I show a derivation of the ChPT based on the Maurer–Cartan 1-form and summarize its predictions. Then, in Section 4, I construct the LSM and review our works accomplished in Refs. [44,70,72], comparing them with the ChPT results. Section 5 is devoted to presenting an extended version of the LSM where, additionally, spin-1 hadrons are incorporated, which is referred to as the extended linear sigma model (eLSM) [71]. Finally, in Section 6, the present article is concluded.

2. QC_2D Lagrangian for Quarks

2.1. Pauli–Gürsey $SU(2N_f)$ Symmetry

The flavor structure, i.e., chiral symmetry, of QC_2D is extended due to the pseudo-reality of the $SU(2)_c$ gauge group, which plays an essential role in describing hadronic excitations in the low-energy region of QC_2D. In this subsection, we explain how such enlarged symmetry emerges by rewriting the QC_2D Lagrangian for quarks.

The Lagrangian for N_f massless quarks interacting with the $SU(2)_c$ gluons is of the form

$$\mathcal{L}_{QC_2D}^{kin} = \bar{\psi} i \slashed{D} \psi \,, \tag{3}$$

where $\psi = (u, d, \cdots)$ is an N_f-components quark field, and the covariant derivative reads $D_\mu \psi = (\partial_\mu - i g_s A_\mu)\psi$ with the $SU(2)_c$ gauge field $A_\mu = A_\mu^a \tau_c^a / 2$ (τ_c^a is the Pauli matrix) and the gauge coupling g_s. To see the chiral structures of the quarks, it is useful to introduce the left-handed and right-handed quark fields, ψ_R and ψ_L, which are eigenstates of the chirality operator γ_5. When employing the Weyl representation, those fields are expressed as $\psi_R = \frac{1+\gamma_5}{2}\psi = (\hat{\psi}_R, \mathbf{0})^T$ and $\psi_L = \frac{1-\gamma_5}{2}\psi = (\mathbf{0}, \hat{\psi}_L)^T$. Hence, Lagrangian (3) is rewritten in terms of the two-component spinors $\hat{\psi}_R$ and $\hat{\psi}_L$ as

$$\mathcal{L}_{QC_2D}^{kin} = \hat{\psi}_R^\dagger i \sigma^\mu (\partial_\mu - i g_s A_\mu)\hat{\psi}_R + \hat{\psi}_L^\dagger i \bar{\sigma}^\mu (\partial_\mu - i g_s A_\mu)\hat{\psi}_L \,, \tag{4}$$

where $\sigma^\mu = (\mathbf{1}, \sigma^i)$ and $\bar{\sigma}^\mu = (\mathbf{1}, -\sigma^i)$ (σ^i is the Pauli matrix inhabiting the spinor space).

The form of Equation (4) is universal for any number of colors. The characteristic feature of the $SU(2)_c$ gauge theory appears when making use of the pseudoreality of the Pauli matrix, $\tau_c^a = -\tau_c^2 (\tau_c^a)^T \tau_c^2$ (and $\sigma^i = -\sigma^2 (\sigma^i)^T \sigma^2$). In fact, these relations enable us to reduce Equation (4) to the following simple form:

$$\mathcal{L}_{QC_2D}^{kin} = \Psi^\dagger i \sigma^\mu \partial_\mu \Psi + g_s \Psi^\dagger \sigma^\mu A_\mu \Psi \,. \tag{5}$$

In this equation, the extended $2N_f$-component quark labeled Ψ is defined by

$$\Psi \equiv (\hat{\psi}_R, \tilde{\hat{\psi}}_L)^T = (\hat{u}_R, \hat{d}_L, \cdots, \tilde{\hat{u}}_L, \tilde{\hat{d}}_L, \cdots)^T \,, \tag{6}$$

with $\hat{\tilde{\psi}}_R = \sigma^2 \tau_c^2 \hat{\psi}_R^*$ and $\hat{\tilde{\psi}}_L = \sigma^2 \tau_c^2 \hat{\psi}_L^*$ being the "conjugate fields" played by the complex conjugate of $\hat{\psi}_L$. The QC$_2$D Lagrangian expressed in terms of Ψ in Equation (5) clearly shows a global symmetry under an $SU(2N_f)$ transformation, generated by

$$\Psi \to g\Psi \quad \text{with} \quad g \in G = SU(2N_f) . \tag{7}$$

Since Ψ is a $2N_f$-component column vector in the (enlarged) flavor space from Equation (6), the symmetry determined by Equation (7) is regarded as an extended version of the $SU(N_f)_L \times SU(N_f)_R$ chiral symmetry. This is sometimes referred to as Pauli–Gürsey $SU(2N_f)$ symmetry [35,36]. Intuitively speaking, the extension of chiral symmetry reflects the blindness of $SU(2)_c$ gluons; quarks and antiquarks belong to $\mathbf{2}$ and $\mathbf{2}^*$ representations of $SU(2)_c$. However, due to the pseudoreality $\mathbf{2} \simeq \mathbf{2}^*$, gluons cannot discriminate quarks and antiquarks. As a result, these states can be treated on an equal footing in a single multiplet, and the flavor structure, i.e., chiral symmetry, is enlarged.

From the above argument, QC$_2$D with massless quarks has been found to possess an $SU(2N_f)$ symmetry generated by Equation (7). Meanwhile, the quark mass term reads

$$\mathcal{L}_{\text{QC}_2\text{D}}^{\text{mass}} = -\frac{1}{2}\left(\Psi^T \sigma^2 \tau_c^2 \mathcal{M}_q \Psi + \text{H.c.}\right) = -\bar{\psi} M_q \psi , \tag{8}$$

where the quark mass matrix in terms of the extended quark multiplet (6) takes the form of the following $2N_f \times 2N_f$ matrix:

$$\mathcal{M}_q = \begin{pmatrix} 0 & -M_q \\ M_q & 0 \end{pmatrix} \tag{9}$$

with $M_q = \text{diag.}(m_u, m_d, \cdots)$. This mass term obviously breaks the $SU(2N_f)$ symmetry, similarly to the (explicit) chiral symmetry breaking in three-color QCD. In particular, when all the quark masses are identical, $m_q \equiv m_u = m_d = \cdots$, the mass term (8) is reduced to

$$\mathcal{L}_{\text{QC}_2\text{D}}^{\text{mass}} = -\frac{m_q}{2}\left(\Psi^T \sigma^2 \tau_c^2 E^T \Psi + \text{H.c.}\right) = -m_q \bar{\psi}\psi , \tag{10}$$

where E is a $2N_f \times 2N_f$ symplectic matrix

$$E = \begin{pmatrix} \mathbf{0} & \mathbf{1} \\ -\mathbf{1} & \mathbf{0} \end{pmatrix} . \tag{11}$$

The operator $\Psi^T \sigma^2 \tau_c^2 E^T \Psi$ is not generally invariant under $g \in G \, (= SU(2N_f))$, but it is only invariant under $h \in H$ belonging to a subgroup of G, which satisfies

$$h^T E h = E . \tag{12}$$

This relation is nothing but the definition of an $Sp(2N_f)$ group. Therefore, $H = Sp(2N_f)$, and the symmetry breaking pattern reads $SU(2N_f) \to Sp(2N_f)$ in this particular case. The number of generators of $SU(2N_f)$ and $Sp(2N_f)$ are $4N_f^2 - 1$ and $N_f(2N_f + 1)$, respectively; thus, the number of NG bosons associated with the breaking of $SU(2N_f) \to Sp(2N_f)$ is

$$4N_f^2 - 1 - N_f(2N_f + 1) = 2N_f^2 - N_f - 1 . \tag{13}$$

As in three-color QCD, $N_f^2 - 1$ pseudoscalar mesons are responsible for the NG bosons, which cannot cover the whole number of Equation (13). That is, in QC$_2$D, $N_f^2 - N_f = 2\,_{N_f}C_2$

NG bosons emerge in addition to the pseudoscalar mesons. These additional NG bosons are played by the flavor-antisymmetric and scalar (anti)diquarks which are in the lightest (anti)baryonic modes, as can be indeed understood by the combination factor $2\,_{N_f}C_2$. The simultaneous emergence of mesonic and (anti)baryonic NG modes also stems from the "blindness" of $SU(2)_c$ gluons.

The $U(1)$ baryon-number and $U(1)$ axial transformations of Ψ are easily understood from definition (6). That is, the upper and lower N_f components of Ψ carry opposite baryon charges and identical axial charges. Thus, when we assign quark-number $+1$ (baryon-number $+1/2$) for $\hat{\psi}$, the resultant $U(1)_B$ transformation law of Ψ reads

$$\Psi \overset{U(1)_B}{\longrightarrow} e^{-i\theta_B J}\Psi \quad \text{with} \quad J = \begin{pmatrix} \mathbf{1} & \mathbf{0} \\ \mathbf{0} & -\mathbf{1} \end{pmatrix}. \tag{14}$$

Similarly,

$$\Psi \overset{U(1)_A}{\longrightarrow} e^{-i\theta_A}\Psi, \tag{15}$$

under the $U(1)$ axial transformation. It should be noted that the $U(1)$ baryon-number transformation (14) belongs to a subgroup of $SU(2N_f)$. Meanwhile, the $U(1)_A$ rotation simply changes the overall phase of Ψ, which is not generated by any of the $SU(2N_f)$ values.

In the following, we restrict ourselves into two-flavor ($N_f = 2$) with an exact isospin symmetry, $m_q \equiv m_u = m_d$, which corresponds to the often-used lattice simulation setup [33], otherwise stated. In this particular case, the symmetry breaking pattern is $SU(4) \to Sp(4)$.

2.2. Algebra of $SU(4)$ and $Sp(4)$

For $N_f = 2$ with isospin symmetry, the Pauli–Gürsey symmetry turns out to be $G = SU(4)$, which contains 15 generators. Since the symmetry breaking pattern is $SU(4) \to Sp(4)$, it is convenient to separate the 15 generators into those belonging to the algebra of $H = Sp(4)$ and $G/H = SU(4)/Sp(4)$: $S^i \in \mathcal{H}$ ($i = 1 - 10$) and $X^a \in \mathcal{G} - \mathcal{H}$ ($a = 1 - 5$). In this paper, we employ

$$S^{i=1-4} = \frac{1}{2\sqrt{2}}\begin{pmatrix} \tau_f^i & 0 \\ 0 & -(\tau_f^i)^T \end{pmatrix}, \quad S^{i=5-10} = \frac{1}{2\sqrt{2}}\begin{pmatrix} 0 & B_f^i \\ (B_f^i)^\dagger & 0 \end{pmatrix}, \tag{16}$$

and

$$X^{a=1-3} = \frac{1}{2\sqrt{2}}\begin{pmatrix} \tau_f^a & 0 \\ 0 & (\tau_f^a)^T \end{pmatrix}, \quad X^{a=4,5} = \frac{1}{2\sqrt{2}}\begin{pmatrix} 0 & D_f^a \\ (D_f^a)^\dagger & 0 \end{pmatrix}, \tag{17}$$

to parametrize them, in which $\tau_f^4 = \mathbf{1}$, $B_f^5 = \mathbf{1}$, $B_f^6 = i\mathbf{1}$, $B_f^7 = \tau_f^3$, $B_f^8 = i\tau_f^3$, $B^9 = \tau_f^1$, $B^{10} = i\tau_f^1$, $D^4 = \tau_f^2$, and $D^5 = i\tau_f^2$, with $\tau_f^{1,2,3}$ being the Pauli matrices acting on the flavor space. The generators belonging to the algebra of the unbroken $Sp(4)$ satisfy

$$S^i E = -E(S^i)^T \quad (S^i \in \mathcal{H}) \tag{18}$$

from Equation (12). Accordingly, the broken generators X^a obey

$$X^a E = E(X^a)^T \quad (X^a \in \mathcal{G} - \mathcal{H}). \tag{19}$$

The above bases are convenient since mesonic and baryonic modes can be properly separated once an effective Lagrangian is constructed.

For later convenience, we further define

$$X^{a=0} = \frac{1}{2\sqrt{2}} \begin{pmatrix} \mathbf{1} & 0 \\ 0 & \mathbf{1} \end{pmatrix} \tag{20}$$

to parametrize the trivial algebra.

2.3. Spurion Fields

Since QC$_2$D with massless quarks preserves the Pauli–Güsey $SU(4)$ symmetry when $N_f = 2$, it is convenient to regard, e.g., quark masses as an external-source contribution breaking the $SU(4)$ symmetry properly. In this subsection, we introduce the so-called *spurion fields* so as to formulate such a systematic inclusion of the breaking effects [37,38].

The source term of QC$_2$D takes the form of

$$\mathcal{L}_{\text{QC}_2\text{D}}^{\text{source}} = -\Psi^T \sigma^2 \tau_c^2 \zeta^\dagger \Psi - \Psi^\dagger \sigma^2 \tau_c^2 \zeta \Psi^* + \Psi^\dagger \sigma_\mu \zeta^\mu \Psi , \tag{21}$$

where the spurion fields ζ $(= -\zeta^T)$ and ζ_μ $(= \zeta_\mu^\dagger)$ transform under local $SU(4)$ transformation as

$$\zeta \to g\zeta g^T , \quad \zeta_\mu \to g\zeta g^\dagger - i\partial_\mu g g^\dagger . \tag{22}$$

In this way, the whole QC$_2$D Lagrangian

$$\mathcal{L}_{\text{QC}_2\text{D}}^q = \mathcal{L}_{\text{QC}_2\text{D}}^{\text{kin}} + \mathcal{L}_{\text{QC}_2\text{D}}^{\text{source}} \tag{23}$$

preserves the local $SU(4)$ symmetry. We note that the spin-1 spurion ζ_μ is introduced as if to be a gauge field with respect to $G = SU(4)$ symmetry. The spurions can be decomposed into real fields s^a, p^a, V_μ^i, and $V_\mu'^a$ as

$$\zeta = \sqrt{2} \sum_{a=0}^{5} (s^a - ip^a) X^a E , \quad \zeta_\mu = 2\sqrt{2} \left(\sum_{i=1}^{10} v_\mu^i S^i - \sum_{a=0}^{5} v_\mu'^a X^a \right) . \tag{24}$$

In the source contribution (21), by replacing the scalar field $s^{a=0}$ with their vacuum expectation value (VEV) as $\langle s^{a=0} \rangle = m_q$ and setting all other fields to be vanishing, one can obtain

$$\mathcal{L}_{\text{QC}_2\text{D}}^{\text{source}} \Big|_{\langle s^0 \rangle = m_q} = -\frac{m_q}{2} \left(\Psi^T \sigma^2 \tau_c^2 E^T \Psi + \text{H.c.} \right) = -m_q \bar{\psi}\psi . \tag{25}$$

This form is, indeed, identical to the mass term in Equation (10). Similarly, a quark chemical potential μ_q can be introduced by choosing the VEV of spin-1 spurions as $\langle v_{\mu=0}^{a=4} \rangle = \mu_q$. Moreover, a diquark source term which leads to condensations of the isospin-singlet and color-singlet scalar diquarks breaking $U(1)_B$ symmetry can also be realized by $\langle p^{a=5} \rangle = j$.

To summarize, within basis (24), when taking the following VEVs,

$$\langle s^{a=0} \rangle = m_q , \quad \langle p^{a=5} \rangle = j , \quad \langle v_{\mu=0}^{i=4} \rangle = \mu_q , \tag{26}$$

the source term (21) is reduced to

$$\begin{aligned}
\mathcal{L}_{\text{QC}_2\text{D}}^{\text{source}} \Big|_{\langle \zeta \rangle, \langle \zeta_\mu \rangle} &= -\sqrt{2}m_q \left(\Psi^T \sigma^2 \tau_c^2 E^T X^0 \Psi + \text{h.c.} \right) - \sqrt{2}j \left(i\Psi^T \sigma^2 \tau_c^2 E^T X^5 \Psi + \text{h.c.} \right) \\
&\quad + 2\sqrt{2}\mu_q \Psi^\dagger S^4 \Psi \\
&= -m_q \bar{\psi}\psi - j \left(-\frac{i}{2} \psi^T C\gamma_5 \tau_c^2 \tau_f^2 \psi + \text{h.c.} \right) + \mu_q \bar{\psi}\gamma^0 \psi ,
\end{aligned} \tag{27}$$

which, indeed, correctly reproduces the quark mass, diquark source, and chemical potential terms.

In addition to the systematic inclusion of the physical parameters as in Equation (27), our spurion-field treatment plays a key role in matching QC$_2$D and low-energy effective models. For instance, taking a functional derivative of Γ_{QC_2D} with respect to s^0 and p^5 and imposing the VEVs (26), one can easily obtain formulas

$$\langle \bar{\psi}\psi \rangle = \left.\frac{\delta\Gamma_{QC_2D}}{-\delta s^0}\right|_{\langle\zeta\rangle,\langle\zeta_\mu\rangle} , \quad \langle \psi\psi \rangle = \left.\frac{\delta\Gamma_{QC_2D}}{-\delta p^0}\right|_{\langle\zeta\rangle,\langle\zeta_\mu\rangle} , \tag{28}$$

respectively, with a shorthand notation of

$$\psi\psi \equiv -\frac{i}{2}\psi^T C\gamma_5 \tau_c^2 \tau_f^2 \psi + \text{h.c.} . \tag{29}$$

Therefore, making use of matching condition (2), the condensates are found to be evaluated within effective models as

$$\langle \bar{\psi}\psi \rangle = \left.\frac{\delta\Gamma_{\text{eff. model}}}{-\delta s^0}\right|_{\langle\zeta\rangle,\langle\zeta_\mu\rangle} , \quad \langle \psi\psi \rangle = \left.\frac{\delta\Gamma_{\text{eff. model}}}{-\delta p^0}\right|_{\langle\zeta\rangle,\langle\zeta_\mu\rangle} . \tag{30}$$

In the same way, any n-point functions of underlying QC$_2$D can be matched with those of the low-energy effective models.

2.4. Ward–Takahashi Identities

Here, we derive the WTIs from symmetry properties of the $SU(4)$ which also play a central role when matching QC$_2$D and the effective models. Here, we only focus on the WTIs connecting spin-0 operators.

Let us define the following spin-0 composite operators:

$$\mathcal{O}_X^a \equiv \Psi^T \sigma^2 \tau_c^2 EX^a \Psi \quad (a = 0-5) . \tag{31}$$

Under the infinitesimal transformation driven by the broken generators X^a, $\Psi \to e^{-i\theta^a X^a}\Psi$, those operators are transformed as

$$\begin{aligned}
\mathcal{O}_X^a \xrightarrow{G/H} \quad & \mathcal{O}_X^a - i\theta^b \Psi^T \sigma^2 \tau_c^2 \left((X^b)^T EX^a + EX^a X^b \right)\Psi \\
= \quad & \mathcal{O}_X^a - \frac{i}{\sqrt{2}}\theta^a \mathcal{O}_X^0 \quad (a = 1-5) ,
\end{aligned} \tag{32}$$

and

$$\begin{aligned}
\mathcal{O}_X^0 \xrightarrow{G/H} \quad & \mathcal{O}_X^0 - i\theta^a \Psi^T \sigma^2 \tau_c^2 \left[(X^a)^T E + EX^a \right] X^0 \Psi \\
= \quad & \mathcal{O}_X^0 - \frac{i}{\sqrt{2}}\theta^a \mathcal{O}_X^a \quad (a = 1-5) ,
\end{aligned} \tag{33}$$

where the algebras in Equation (19) and $\{X^a, X^b\} = \delta^{ab}E/4$ $(a, b = 1-5)$ are used. Similarly, under $U(1)_B$ transformation $\Psi \to e^{-i\theta_B J}\Psi$, one can see

$$\mathcal{O}_X^a \xrightarrow{U(1)_B} \mathcal{O}_X^a - i\theta_B \Psi^T \sigma^2 \tau_c^2 \{J, EX^a\}\Psi = \begin{cases} \mathcal{O}_X^a & (a = 0-3) \\ \mathcal{O}_X^4 + 2\theta_B \mathcal{O}_X^5 & (a = 4) \\ \mathcal{O}_X^5 - 2\theta_B \mathcal{O}_X^4 & (a = 5) \end{cases} . \tag{34}$$

Although the composite operators (31) exhibit concise transformation properties, they include positive-parity and negative-parity states collectively and are not useful as building blocks of the physical states. For this reason, we also define

$$
\begin{aligned}
\mathcal{O}_\sigma &\equiv \bar{\psi}\psi = -\sqrt{2}\mathcal{O}_X^0 - \sqrt{2}\mathcal{O}_X^{\dagger 0}, \\
\mathcal{O}_{a_0}^a &\equiv \bar{\psi}\tau_f^a\psi = -\sqrt{2}\mathcal{O}_X^a - \sqrt{2}\mathcal{O}_X^{\dagger a} \quad (a = 1-3), \\
\mathcal{O}_\eta &\equiv \bar{\psi}i\gamma_5\psi = -\sqrt{2}i\mathcal{O}_X^0 + \sqrt{2}i\mathcal{O}_X^{\dagger 0}, \\
\mathcal{O}_\pi^a &\equiv \bar{\psi}i\gamma_5\tau_f^a\psi = -\sqrt{2}i\mathcal{O}_X^a + \sqrt{2}i\mathcal{O}_X^{\dagger a} \quad (a = 1-3),
\end{aligned}
\tag{35}
$$

for mesonic operators, and

$$
\begin{aligned}
\mathcal{O}_{B_4} &\equiv \frac{1}{2}\psi^T C\gamma_5\tau_c^2\tau_f^2\psi + \text{h.c.} = -\sqrt{2}i\mathcal{O}_X^4 + \sqrt{2}i\mathcal{O}_X^{\dagger 4}, \\
\mathcal{O}_{B_5} &\equiv -\frac{i}{2}\psi^T C\gamma_5\tau_c^2\tau_f^2\psi + \text{h.c.} = -\sqrt{2}i\mathcal{O}_X^5 + \sqrt{2}i\mathcal{O}_X^{\dagger 5}, \\
\mathcal{O}_{B_4'} &\equiv -\frac{i}{2}\psi^T C\tau_c^2\tau_f^2\psi + \text{h.c.} = -\sqrt{2}\mathcal{O}_X^4 - \sqrt{2}\mathcal{O}_X^{\dagger 4}, \\
\mathcal{O}_{B_5'} &\equiv -\frac{1}{2}\psi^T C\tau_c^2\tau_f^2\psi + \text{h.c.} = -\sqrt{2}\mathcal{O}_X^5 - \sqrt{2}\mathcal{O}_X^{\dagger 5},
\end{aligned}
\tag{36}
$$

for baryonic ones. Their transformation laws are easily seen from Equations (32)–(34).

Inserting the VEVs (26) of the spurion fields, the QC$_2$D Lagrangian (23) now takes the form of

$$
\mathcal{L}_{QC_2D}^q = \Psi^\dagger i\sigma_\mu \mathcal{D}^\mu \Psi + \sqrt{2}m_q\left(\mathcal{O}_X^0 + \mathcal{O}_X^{0\dagger}\right) + \sqrt{2}j\left(i\mathcal{O}_X^5 - i\mathcal{O}_X^{5\dagger}\right),
\tag{37}
$$

with $\mathcal{D}_\mu\Psi = (\partial_\mu - ig_sA_\mu - i\mu_q J)\Psi$ and the composite operators being defined by Equation (31). Under the local transformation generated by $X^a \in \mathcal{G} - \mathcal{H}$ ($a = 1-5$), this Lagrangian transforms as

$$
\mathcal{L}_{QC_2D}^q \overset{G/H}{\to} \mathcal{L}_{QC_2D}^q - \theta^a\left[D_\mu j_X^{\mu a} - m_q\left(i\mathcal{O}_X^a - i\mathcal{O}_X^{a\dagger}\right) + j^a\delta^{5a}\left(\mathcal{O}_X^0 + \mathcal{O}_X^{0\dagger}\right)\right],
\tag{38}
$$

in which we have made use of the integration by parts to collectively treat the corrections. The broken current $j_X^{\mu a}$ is given by

$$
j_X^{\mu a} = \Psi^\dagger \sigma^\mu X^a \Psi,
\tag{39}
$$

with the covariant derivative of the form

$$
D_\mu j_X^{\mu a} = \partial_\mu j_X^a - i\mu_q\delta_{\mu 0}\Psi^\dagger[X^a, J] = \begin{cases} \partial_\mu j_X^{\mu a} & (a = 1-3) \\ \partial_\mu j_X^{\mu 4} + 2\mu_q\delta_{\mu 0}j_X^{\mu 5} & (a = 4) \\ \partial_\mu j_X^{\mu 5} - 2\mu_q\delta_{\mu 0}j_X^{\mu 4} & (a = 5) \end{cases}.
\tag{40}
$$

Here, let us focus on an arbitrary functional which takes the form of

$$
\mathcal{I}[\hat{\mathcal{O}}(y)] \equiv \int [d\bar{\psi}d\psi][dA]\hat{\mathcal{O}}(y)e^{i\int d^4x\mathcal{L}_{QC_2D}^q}.
\tag{41}
$$

Assuming that the G/H transformation law of the operator $\hat{\mathcal{O}}$ reads $\hat{\mathcal{O}} \overset{G/H}{\to} \hat{\mathcal{O}} + \theta^a\delta^a\hat{\mathcal{O}}$, the invariance of the functional $\mathcal{I}[\hat{\mathcal{O}}(y)]$ yields the following identity for Green's functions:

$$
\langle\delta^a\hat{\mathcal{O}}\rangle\delta^{ab}\delta(x) = i\left\langle \text{T}^*\left[\partial_\mu j_X^{\mu b} + m_q\left(i\mathcal{O}_X^b - i\mathcal{O}_X^{b\dagger}\right) + \frac{j}{\sqrt{2}}\delta^{b5}\mathcal{O}_\sigma\right](x)\hat{\mathcal{O}}(0)\right\rangle.
\tag{42}
$$

In this identity, we have set $y = 0$, and the symbol T* stands for the time-ordering operator but commutes with any derivatives that maintain the explicit Lorentz covariance of the path-integral formulation. Therefore, choosing $\mathcal{O}_\pi^a$, $\mathcal{O}_{B_4}$, $\mathcal{O}_{B_5}$, and $\mathcal{O}_\sigma$ for $\hat{\mathcal{O}}$, from Equation (42), we arrive at the following WTIs:

$$\langle \mathcal{O}_\sigma \rangle \delta^{ab} \delta(x) = \sqrt{2} \langle \mathrm{T}^* i\partial_\mu^x j_X^{\mu b}(x) \mathcal{O}_\pi^a(0) \rangle - im_q \langle \mathrm{T} \mathcal{O}_\pi^b(x) \mathcal{O}_\pi^a(0) \rangle \quad (a, b = 1 - 3), \tag{43}$$

$$\langle \mathcal{O}_\sigma \rangle \delta(x) = \sqrt{2} \langle \mathrm{T}^* i D_\mu^x j_X^{\mu 4}(x) \mathcal{O}_{B_4}(0) \rangle - im_q \langle \mathrm{T} \mathcal{O}_{B_4}(x) \mathcal{O}_{B_4}(0) \rangle, \tag{44}$$

$$\langle \mathcal{O}_\sigma \rangle \delta(x) = \sqrt{2} \langle \mathrm{T}^* i D_\mu^x j_X^{\mu 5}(x) \mathcal{O}_{B_5}(0) \rangle - im_q \langle \mathrm{T} \mathcal{O}_{B_5}(x) \mathcal{O}_{B_5}(0) \rangle + ij \langle \mathrm{T} \mathcal{O}_\sigma(x) \mathcal{O}_{B_5}(0) \rangle, \tag{45}$$

and

$$-\langle \mathcal{O}_{B_5} \rangle \delta(x) = \sqrt{2} \langle \mathrm{T}^* i D_\mu^x j_X^{\mu 5}(x) \mathcal{O}_\sigma(0) \rangle - im_q \langle \mathrm{T} \mathcal{O}_{B_5}(x) \mathcal{O}_\sigma(0) \rangle + ij \langle \mathrm{T} \mathcal{O}_\sigma(x) \mathcal{O}_\sigma(0) \rangle, \tag{46}$$

respectively, with the help of the transformation laws presented in Equations (32) and (33).

Likewise, the local $U(1)_B$ transformation law of the Lagrangian (37) reads

$$\mathcal{L}_{\mathrm{QC_2D}}^q \overset{U(1)_B}{\to} \mathcal{L}_{\mathrm{QC_2D}}^q - \theta_B \left[\partial_\mu j_B^\mu + 2\sqrt{2} j (i\mathcal{O}_X^4 - i\mathcal{O}_X^{\dagger 4}) \right] \tag{47}$$

from $\Psi \to e^{-i\theta_B J} \Psi$, with $j_B^\mu = \Psi^\dagger \sigma^\mu J \Psi$ being the baryon-number current. Hence, tracing the same procedure below Equation (41),

$$\langle \delta_B \hat{\mathcal{O}} \rangle \delta(x) = i \left\langle \mathrm{T}^* \left[\partial_\mu j_B^\mu - 2j \mathcal{O}_{B_4} \right](x) \hat{\mathcal{O}}(0) \right\rangle \tag{48}$$

is derived, where the transformed part, $\delta_B \hat{\mathcal{O}}$, has been defined through $\hat{\mathcal{O}} \overset{U(1)_B}{\to} \hat{\mathcal{O}} + \theta_B \delta_B \hat{\mathcal{O}}$. Taking $\mathcal{O}_{B_4}$ for $\hat{\mathcal{O}}$ in this identity, one can find the following WTI in terms of $U(1)_B$ symmetry:

$$2 \langle \mathcal{O}_{B_5} \rangle \delta(x) = i\partial_\mu^x \langle \mathrm{T} j_B^\mu(x) \mathcal{O}_{B_4}(0) \rangle - 2ij \langle \mathrm{T} \mathcal{O}_{B_4}(x) \mathcal{O}_{B_4}(0) \rangle. \tag{49}$$

It should be noted that all the WTIs derived in this subsection are valid at any temperature and density since only the symmetry properties of the functional (41) are utilized in the derivations.

2.5. Gell–Mann–Oakes–Renner Relationships with the Diquark Source

In Section 2.4, the WTIs connecting the chiral and diquark condensates to the particular two-point functions were derived from the appropriate invariance of the path-integral formalism. Here, based on the identities, we present the so-called Gell–Mann–Oakes–Renner (GOR) relationships [75] in the presence of the diquark source j, which is valid as long as we stick to low-energy QC_2D.

First, we focus on the pion sector (43) that is separated from the baryonic sectors and explicit chemical potential effects. By inserting only a pion one-particle state

$$\int \frac{d^3p}{(2\pi)^3 2E_\pi} |\pi^c(\boldsymbol{p})\rangle \langle \pi^c(\boldsymbol{p})| \tag{50}$$

as a part of the complete set (E_π is a pion dispersion relation), the first term in the RHS of Equation (43) can be simplified to be (T is the ordinary time-ordering operator)

$$\langle T^* i\partial^x_\mu j^{\mu b}_X(x)\mathcal{O}^a_\pi(0)\rangle \sim T\int \frac{d^3p}{(2\pi)^3 2E_\pi} if_\pi p^2 \mathcal{A}_{\pi\pi} e^{-ip_\pi \cdot x} , \tag{51}$$

where we assume that the amplitude can be evaluated as

$$\begin{aligned}
\langle 0|j^{\mu b}_X(x)|\pi^a(\boldsymbol{p})\rangle &= if_\pi p^\mu \delta^{ab} e^{-ip_\pi \cdot x} , \\
\langle 0|\mathcal{O}^b_\pi(x)|\pi^a(\boldsymbol{p})\rangle &= \mathcal{A}_{\pi\pi} \delta^{ab} e^{-ip_\pi \cdot x} ,
\end{aligned} \tag{52}$$

with a pion decay constant f_π and a $\boldsymbol{p}$-independent matrix element $\mathcal{A}_{\pi\pi}$. The momentum p^μ_π is defined by $p^\mu_\pi = (E_\pi, \boldsymbol{p})$. Thus, the matrix element (51) is reduced to

$$\langle T^* i\partial^x_\mu j^{\mu b}_X(x)\mathcal{O}^a_\pi(0)\rangle \sim -\int \frac{d^4p}{(2\pi)^4} \frac{f_\pi p^2 \mathcal{A}_{\pi\pi}}{p_0^2 - E_\pi^2} e^{-ip\cdot x} . \tag{53}$$

In a similar way, the second term of the RHS of Equation (43) reads

$$\langle T\mathcal{O}^b_\pi(x)\mathcal{O}^a_\pi(0)\rangle \sim T\int \frac{d^3p}{(2\pi)^3 2E_\pi} |\mathcal{A}_{\pi\pi}|^2 e^{-ip_\pi \cdot x} = \int \frac{d^4p}{(2\pi)^4} \frac{i|\mathcal{A}_{\pi\pi}|^2}{p_0^2 - E_\pi^2} e^{-ip\cdot x} , \tag{54}$$

and, hence, one can arrive at ($\mathcal{A}^*_{\pi\pi} = \mathcal{A}_{\pi\pi}$)

$$\langle \mathcal{O}_\sigma \rangle = -\frac{\sqrt{2}f_\pi p^2 \mathcal{A}_{\pi\pi}}{p_0^2 - E_\pi^2} + \frac{m_q \mathcal{A}^2_{\pi\pi}}{p_0^2 - E_\pi^2} . \tag{55}$$

When taking $p_0 \to 0$ and $p_0 \to E_\pi$ after choosing the rest frame $\boldsymbol{p} = \boldsymbol{0}$, two equations,

$$\langle \mathcal{O}_\sigma \rangle = -\frac{m_q}{m_\pi^2} \mathcal{A}^2_{\pi\pi} , \quad 0 = -\sqrt{2}f_\pi m_\pi^2 \mathcal{A}_{\pi\pi} + m_q \mathcal{A}^2_{\pi\pi} , \tag{56}$$

are obtained, with $m_\pi \equiv E_\pi|_{\boldsymbol{p}=\boldsymbol{0}}$ being the pion mass. Therefore, eliminating the matrix element $\mathcal{A}_{\pi\pi}$, we finally find

$$f_\pi^2 m_\pi^2 = -\frac{m_q \langle \mathcal{O}_\sigma \rangle}{2} , \tag{57}$$

which is nothing but the familiar GOR relation. The factor $1/2$ in the RHS is due to the normalization of f_π in QC$_2$D, as will be explained in Section 2.6. It should be noted that this relationship holds at any density as long as the one-pion saturation of the complete set and momentum independence of $\mathcal{A}_{\pi\pi}$ are reasonably satisfied.

Next, we move on to the baryonic sector. The μ_q independence of the GOR relationship for the pion sector is due to decouplings from the baryonic sector; meanwhile, the baryonic WTIs are easily affected by μ_q and contaminations from $\mathcal{O}_\sigma$ due to the $U(1)_B$ violation too. In order to reduce these difficulties, here, we restrict ourselves to $\mu_q = 0$. In this case, the WTI for $\mathcal{O}_{B_4}$, Equation (44), coincides with the pion's. Additionally, due to the charge-conjugation symmetry, $\mathcal{O}_{B_4}$ is always separated from $\mathcal{O}_{B_5}$ and $\mathcal{O}_\sigma$. (Only $\mathcal{O}_{B_4}$ carries $C = -1$, while $\mathcal{O}_{B_5}$ and $\mathcal{O}_\sigma$ carry $C = +1$.) Thus, the GOR relation from Equation (44) coincides with that of Equation (57), from which the mass of B_4 is equal to the pion mass. On the other hand, the WTI for $\mathcal{O}_{B_5}$ is still complicated due to mixings from $\mathcal{O}_\sigma$, stemming from the $U(1)_B$ violation.

The WTIs for $\mathcal{O}_{B_5}$ and $\mathcal{O}_\sigma$ are combined into a single relationship, as shown below. By defining the mass eigenoperators $\mathcal{O}_{\tilde{B}_5}$ and $\mathcal{O}_{\tilde{\sigma}}$ through

$$
\begin{pmatrix} \mathcal{O}_{\tilde{B}_5} \\ \mathcal{O}_{\tilde{\sigma}} \end{pmatrix} = \begin{pmatrix} \cos\theta & -\sin\theta \\ \sin\theta & \cos\theta \end{pmatrix} \begin{pmatrix} \mathcal{O}_{B_5} \\ \mathcal{O}_\sigma \end{pmatrix} ,
\tag{58}
$$

overlaps of the operators $\mathcal{O}_{B_5}$ and $\mathcal{O}_\sigma$ between the $\tilde{B}_5$ state and the vacuum can be evaluated to be

$$
\begin{aligned}
\langle 0|\mathcal{O}_{B_5}|\tilde{B}_5(\boldsymbol{p})\rangle &= \cos\theta\langle 0|\mathcal{O}_{\tilde{B}_5}|\tilde{B}_5(\boldsymbol{p})\rangle = \mathcal{A}_{\tilde{B}_5\tilde{B}_5}\cos\theta , \\
\langle 0|\mathcal{O}_\sigma|\tilde{B}_5(\boldsymbol{p})\rangle &= -\sin\theta\langle 0|\mathcal{O}_{\tilde{B}_5}|\tilde{B}_5(\boldsymbol{p})\rangle = -\mathcal{A}_{\tilde{B}_5\tilde{B}_5}\sin\theta ,
\end{aligned}
\tag{59}
$$

where $\mathcal{A}_{\tilde{B}_5\tilde{B}_5}$ has been defined similarly to Equation (52). Then, introducing the decay constant f_5 by

$$
\langle 0|j_X^{\mu 5}(0)|\tilde{B}_5(\boldsymbol{p})\rangle = if_5 p^\mu ,
\tag{60}
$$

from Equations (45) and (46), one can derive

$$
\begin{aligned}
\langle\mathcal{O}_\sigma\rangle &= -\frac{\sqrt{2}f_5 p^2 \mathcal{A}_{\tilde{B}_5\tilde{B}_5}\cos\theta}{p_0^2 - E_{\tilde{B}_5}^2} + \frac{m_q\mathcal{A}_{\tilde{B}_5\tilde{B}_5}^2\cos^2\theta}{p_0^2 - E_{\tilde{B}_5}^2} + \frac{j\mathcal{A}_{\tilde{B}_5\tilde{B}_5}^2\sin\theta\cos\theta}{p_0^2 - E_{\tilde{B}_5}^2} , \\
\langle\mathcal{O}_{B_5}\rangle &= -\frac{\sqrt{2}\mathcal{A}_{\tilde{B}_5\tilde{B}_5}f_5 p^2 \sin\theta}{p_0^2 - E_{\tilde{B}_5}^2} + \frac{m_q\mathcal{A}_{\tilde{B}_5\tilde{B}_5}^2\sin\theta\cos\theta}{p_0^2 - E_{\tilde{B}_5}^2} + \frac{j\mathcal{A}_{\tilde{B}_5\tilde{B}_5}^2\sin^2\theta}{p_0^2 - E_{\tilde{B}_5}^2} ,
\end{aligned}
\tag{61}
$$

as siblings of Equation (55). We note that all transitions to $|\tilde{\sigma}(\boldsymbol{p})\rangle$ have been omitted in the derivation since only the (approximate) NG bosons are assumed to saturate the low-energy physics of QC$_2$D. Taking $p_0 \to 0$ and $p_0 \to m_\pi$ at the rest frame $\boldsymbol{p} = \boldsymbol{0}$ (the mass of $\tilde{B}_5$ is identical to the pion mass) in Equation (61),

$$
\mathcal{A}_{\tilde{B}_5\tilde{B}_5} = -\frac{\langle\mathcal{O}_\sigma\rangle}{\sqrt{2}f_5\cos\theta} = -\frac{\langle\mathcal{O}_{B_5}\rangle}{\sqrt{2}f_5\sin\theta}
\tag{62}
$$

is found; so, inserting this relation into either part of Equation (61) at $p \to 0$ yields

$$
f_5^2 m_\pi^2 = -\frac{m_q\langle\mathcal{O}_\sigma\rangle}{2} - \frac{j\langle\mathcal{O}_{B_5}\rangle}{2} .
\tag{63}
$$

Finally, the WTI (49) related to $U(1)_B$ symmetry is easily derived to be

$$
\left(\frac{f_B}{2\sqrt{2}}\right)^2 m_\pi^2 = -\frac{j\langle\mathcal{O}_{B_5}\rangle}{2} ,
\tag{64}
$$

where the decay constant associated with the baryon-number current f_B has been defined through

$$
\langle 0|j_B^\mu(0)|B_4(\boldsymbol{p})\rangle = if_B p^\mu .
\tag{65}
$$

In summary, the GOR relation with respect to the broken current $j_X^{\mu a}$ and the $U(1)$ baryon-number current j_B^μ are obtained as

$$f_\pi^2 m_\pi^2 = -\frac{m_q \langle \bar\psi \psi \rangle}{2} \quad \text{(at any } \mu_q \text{)} , \tag{66}$$

$$f_5^2 m_\pi^2 = -\frac{m_q \langle \bar\psi \psi \rangle}{2} - \frac{j \langle \psi \psi \rangle}{2} \quad \text{(only at } \mu_q = 0 \text{)} , \tag{67}$$

$$\left(\frac{f_B}{2\sqrt{2}} \right)^2 m_\pi^2 = -\frac{j \langle \psi \psi \rangle}{2} \quad \text{(only at } \mu_q = 0 \text{)} , \tag{68}$$

where the decay constants are introduced from Equations (52), (60), and (65). Additionally, we have used $\mathcal{O}_\sigma = \bar\psi \psi$ and shorthand notation for the diquark operator $\mathcal{O}_{B_5} = \psi \psi$.

2.6. Comment on the Decay Constant f_π

In Section 2.5, the pion decay constant f_π was introduced through matrix element (52) associated with the broken current $j_X^{\mu a}$ and one-pion state $|\pi^a(\boldsymbol{p})\rangle$. The broken current for the pion sector can be expressed in terms of the ordinary quark field ψ as

$$j_X^{\mu a} = \Psi^\dagger \sigma^\mu X^a \Psi = \frac{1}{\sqrt{2}} \bar\psi \gamma^\mu \gamma_5 T_f^a \psi = j_5^{\mu a} \quad (a = 1 - 3) , \tag{69}$$

where $T_f^a = \tau_f^a / 2$ and the familiar axial current $j_5^{\mu a} \equiv \bar\psi \gamma^\mu \gamma_5 T_f^a \psi$ have been defined. Then, the matrix element is rewritten into

$$\langle 0 | j_X^{\mu a}(x) | \pi^b(\boldsymbol{p}) \rangle = \frac{1}{\sqrt{2}} \langle 0 | j_5^{\mu a}(x) | \pi^b(\boldsymbol{p}) \rangle . \tag{70}$$

The decay constant in three-color QCD, $f_\pi^{N_c=3} = 93\,\text{MeV}$, is introduced with respect to the familiar broken current $j_5^{\mu a}$ though

$$\langle 0 | j_5^{\mu a}(x) | \pi^b(\boldsymbol{p}) \rangle = i f_\pi^{N_c=3} p^\mu \delta^{ab} \mathrm{e}^{-i p_\pi \cdot x} . \tag{71}$$

Hence, Equation (70) can be expressed in terms of $f_\pi^{N_c=3}$ as

$$\langle 0 | j_X^{\mu a}(x) | \pi^b(\boldsymbol{p}) \rangle = \frac{i}{\sqrt{2}} f_\pi^{N_c=3} p^\mu \delta^{ab} \mathrm{e}^{-i p_\pi \cdot x} , \tag{72}$$

and comparing this equation with the QC$_2$D definition in Equation (52), one can find

$$f_\pi = \frac{1}{\sqrt{2}} f_\pi^{N_c=3} . \tag{73}$$

Equation (73) implies that the decay constant in QC$_2$D is different from the three-color QCD one by a factor $1/\sqrt{2}$. Within chiral effective models such as the ChPT, LSM, and NJL model in QC$_2$D, the decay constant is, of course, defined through the broken current associated with the generator X^a, which corresponds not to $f_\pi^{N_c=3}$ but f_π.

3. Chiral Perturbation Theory

3.1. Model Construction Based on the Maurer–Cartan 1-Form

Among hadron effective models, the ChPT which treats NG bosons in association with a certain symmetry breaking is one of the most powerful and standard models due to its systematic low-energy expansion. Thus, in this subsection, we explain derivation of the ChPT in QC$_2$D in terms of the so-called Maurer–Cartan 1-form [76].

Let us introduce the following representative which parametrizes the coset space $G/H = SU(4)/Sp(4)$,

$$\xi = \exp(i\pi^a X^a / f_0) \,, \tag{74}$$

where the π^as can be regarded as the NG bosons: three pions, a diquark, and an antidiquark. Additionally, f_0 is a parameter with a mass dimension of $+1$, which corresponds to the pion decay constant in the lowest order of ChPT, at a vanishing μ_q.

From the properties of the coset and representative, one can choose that the ξ defined in Equation (74) be transformed under the global $SU(4)$ transformation as [76]

$$\xi \rightarrow g\xi h^\dagger(g, \pi) \,. \tag{75}$$

We note that $h(g, \pi)$ must be a function of g and π for which the representative ξ correctly transforms. Here, for later convenience, we introduce the Maurer–Cartan 1-form

$$\alpha_\mu \equiv i^{-1}\partial_\mu \xi^\dagger \xi \,. \tag{76}$$

This 1-form is indeed useful to construct a Lagrangian from the viewpoint of low-energy expansion since it includes one derivative, and the G-transformation law is simply generated by $h(g, \pi)$:

$$\alpha_\mu \rightarrow h(g, \pi)\alpha_\mu h^\dagger(g, \pi) - i\partial_\mu h(g, \pi)h^\dagger(g, \pi) \,. \tag{77}$$

The 1-form (76) generally belongs to the algebra of both $\mathcal{H}$ and $\mathcal{G} - \mathcal{H}$, so we try to separate them. The decomposition is performed by introducing a sibling of ξ as

$$\tilde{\xi} \equiv E^T \xi^* E \,. \tag{78}$$

In fact, when defining

$$\begin{aligned}
\alpha_{\perp,\mu} &= \frac{1}{2i}(\partial_\mu \xi^\dagger \xi - \partial_\mu \tilde{\xi}^\dagger \tilde{\xi}) \,, \\
\alpha_{\parallel,\mu} &= \frac{1}{2i}(\partial_\mu \xi^\dagger \xi + \partial_\mu \tilde{\xi}^\dagger \tilde{\xi}) \,,
\end{aligned} \tag{79}$$

so as to satisfy $a_\mu = a_{\perp,\mu} + a_{\parallel,\mu}$, those are expanded as

$$\alpha_{\perp,\mu} = -\frac{\partial_\mu \pi^a}{f_0}X^a + \cdots \,, \quad \alpha_{\parallel,\mu} = \frac{\partial_\mu \pi^a \pi^b}{2if_0^2}[X^a, X^b] + \cdots \,. \tag{80}$$

Here, $[X^a, X^b]E = -E[X^a, X^b]^T$ follows from Equation (19); then, the commutator $[X^a, X^b]$ is understood to belong to the algebra $\mathcal{H}$ from definition (18). In this way, we can conclude that

$$\alpha_{\perp,\mu} \in \mathcal{G} - \mathcal{H} \quad \text{while} \quad \alpha_{\parallel,\mu} \in \mathcal{H} \,. \tag{81}$$

Additionally, the transformation laws of $\alpha_{\perp,\mu}$ and $\alpha_{\parallel,\mu}$ under $G = SU(4)$ read

$$\begin{aligned}
\alpha_{\perp,\mu} &\rightarrow h(g, \pi)\alpha_{\perp,\mu}h^\dagger(g, \pi) \,, \\
\alpha_{\parallel,\mu} &\rightarrow h(g, \pi)\alpha_{\parallel,\mu}h^\dagger(g, \pi) - i\partial_\mu h(g, \pi)h^\dagger(g, \pi) \,,
\end{aligned} \tag{82}$$

respectively, with the help of the following property:

$$\tilde{\xi} \rightarrow E^T g^* \xi^* h^T(g, \pi) E = E^T g^* E \tilde{\xi} h^\dagger(g, \pi) \tag{83}$$

following from the algebras in Equations (18) and (19).

Based on the above building blocks, the $SU(4)$-invariant ChPT Lagrangian of $\mathcal{O}(p^2)$ is constructed as

$$\mathcal{L}_{\text{ChPT}}^{\mathcal{O}(p^2)} = f_0^2 \text{tr}[\alpha_{\perp,\mu} \alpha_\perp^\mu] + f_0^2 \text{tr}[\hat{\zeta} + \hat{\zeta}^\dagger] \, , \tag{84}$$

where we have defined

$$\hat{\zeta} = B_0 \xi^\dagger \zeta E^T \tilde{\xi} \tag{85}$$

with B_0 being a constant with the mass dimension $+1$, the $SU(4)$ transformation law of which is

$$\hat{\zeta} \rightarrow h(g, \pi) \hat{\zeta} h^\dagger(g, \pi) \, . \tag{86}$$

The field ζ in Equation (85) is the spin-0 spurion field, which is replaced by its VEV to incorporate, e.g., the quark mass m_q effect in the end, as explained in Section 2.3.

Our main aim to employ the ChPT is to explore the low-energy physics of cold and dense QC$_2$D, so we need to incorporate a quark chemical potential. The chemical potential is introduced systematically by gauging Equation (84) with respect to $SU(4)$ to incorporate the spin-1 spurion field ζ_μ, and replacing it by the VEV with $\langle v_{\mu=0}^{i=4} \rangle = \mu_q$ from Equations (24) and (26). Then, in the following analysis, we will use

$$\alpha_{\perp,\mu} = \frac{1}{2i}(D_\mu \xi^\dagger \xi - D_\mu \tilde{\xi}^\dagger \tilde{\xi}) \tag{87}$$

as the 1-form, where the covariant derivative reads

$$D_\mu \xi^\dagger \equiv \partial_\mu \xi^\dagger + i\xi^\dagger \zeta_\mu \, , \quad D_\mu \tilde{\xi}^\dagger \equiv \partial_\mu \tilde{\xi}^\dagger - i\tilde{\xi}^\dagger E^T \zeta_\mu^T E \, , \tag{88}$$

with $\zeta_\mu \rightarrow \langle \zeta_\mu \rangle = \mu_q \delta_{\mu 0} J$, from the transformation properties (75) and (83). On the other hand, for a while, we ignore the diquark source j.

3.2. ChPT in the Hadronic Phase

In Section 3.1, we constructed the ChPT Lagrangian of $\mathcal{O}(p^2)$ in terms of the Maurer–Cartan 1-form in Equation (84). Defining $U = \xi E^T \xi^T$, the Lagrangian is rewritten to

$$\mathcal{L}_{\text{ChPT}}^{\mathcal{O}(p^2)} = \frac{f_0^2}{4} \text{tr}[D_\mu U^\dagger D^\mu U] + \text{tr}[U\zeta^\dagger + U^\dagger \zeta] \, , \tag{89}$$

which is, indeed, identical to the Lagrangian invented by Kogut et. al. [39,40]. In this equation, the covariant derivative reads

$$D_\mu U = \partial_\mu U - i\zeta_\mu U - iU\zeta_\mu^T \, . \tag{90}$$

Setting $\langle \pi^a \rangle = 0$, or $\langle \xi \rangle = 1$, one finds $\langle U \rangle = E^T$ from its definition. This VEV must be associated with the ground-state configuration of low-energy QC$_2$D, i.e., the chiral condensate $\langle \bar{\psi}\psi \rangle$ in the hadronic phase, as long as the diquark source j is switched off and μ_q is adequately small. In other words, conceptionally, the VEV takes the form of $\langle U \rangle \propto \langle \bar{\psi}\psi \rangle E^T$ for which the remaining $Sp(4)$ symmetry of QC$_2$D is properly built in.

To gain more insights into this structure, we introduce a quark bilinear Φ_{ij} with flavor indices uncontracted as

$$\Phi_{ij} \equiv \Psi_j^T \sigma^2 \tau_c^2 \Psi_i \,. \tag{91}$$

Using definition (6), one can easily show that the VEV of a scalar operator $\langle \bar{\psi}\psi \rangle$ can be embedded into $\langle \Phi \rangle$ as $\langle \Phi \rangle = -(1/4)\langle \bar{\psi}\psi \rangle E^T$, and hence, the VEV of Φ corresponds to the correct ground-state configuration of $\langle U \rangle$: $\langle U \rangle \propto \langle \Phi \rangle$. This fact implies that when U is expanded up to $\mathcal{O}(\pi)$, its quark-bilinear representation is identical to the linear operator Φ. In this linearization U reads

$$U \approx E^T + \frac{i}{\sqrt{2}f_0} \begin{pmatrix} 0 & \pi^5 - i\pi^4 & -\pi^3 & -(\pi^1 - i\pi^2) \\ -(\pi^5 - i\pi^4) & 0 & -(\pi^1 + i\pi^2) & \pi^3 \\ \pi^3 & \pi^1 + i\pi^2 & 0 & \pi^5 + i\pi^4 \\ \pi^1 - i\pi^2 & -\pi^3 & -(\pi^5 + i\pi^4) & 0 \end{pmatrix}. \tag{92}$$

Meanwhile, pionic and baryonic bilinear operators ($\tau_f^\pm = \tau_f^1 \pm i\tau_f^2$)

$$\pi^\pm \sim \frac{1}{\sqrt{2}} \bar{\psi} i\gamma_5 \tau_f^\mp \psi \,, \quad \pi^0 \sim \bar{\psi} i\gamma_5 \tau_f^3 \psi \,,$$

$$B \sim -\frac{i}{\sqrt{2}} \psi^T C\gamma_5 \tau^2 \tau_f^2 \psi \,, \quad \bar{B} \sim -\frac{i}{\sqrt{2}} \psi^\dagger C\gamma_5 \tau^2 \tau_f^2 \psi^* \,, \tag{93}$$

are involved in Φ as (regardless of the normalization)

$$\Phi \sim \begin{pmatrix} 0 & \sqrt{2}iB & -i\pi^0 & -\sqrt{2}i\pi^+ \\ -\sqrt{2}iB & 0 & -\sqrt{2}i\pi^- & i\pi^0 \\ i\pi^0 & \sqrt{2}i\pi^- & 0 & \sqrt{2}i\bar{B} \\ \sqrt{2}i\pi^+ & -i\pi^0 & -\sqrt{2}i\bar{B} & 0 \end{pmatrix}, \tag{94}$$

from Equation (91). Therefore, comparing the second term of Equations (92) and (94) enables us to identify pions and (anti)diquarks as

$$\pi^\pm = \frac{\pi^1 \mp i\pi^2}{\sqrt{2}} \,, \quad \pi^0 = \pi^3 \,, \quad B = \frac{\pi^5 - i\pi^4}{\sqrt{2}} \,, \quad \bar{B} = \frac{\pi^5 + i\pi^4}{\sqrt{2}} \,, \tag{95}$$

by choosing normalizations appropriately. We note that the E^T part in Equation (92) simply denotes the vacuum configuration in the hadronic phase: $\langle U \rangle = E^T$.

By reading off the quadratic term of π^a ($a = 1$–3) in the ChPT Lagrangian (89), the pion masses are derived to be

$$\left(m_\pi^{(\mathrm{H})}\right)^2 = 2B_0 m_q \,; \tag{96}$$

meanwhile, the diquark and antidiquark masses read

$$m_B^{(\mathrm{H})} = m_\pi^{(\mathrm{H})} - 2\mu_q \,, \quad m_{\bar{B}}^{(\mathrm{H})} = m_\pi^{(\mathrm{H})} + 2\mu_q \,. \tag{97}$$

In these equations, the superscript (H) has been attached to emphasize that the mass formulas are valid only in the hadronic phase.

3.3. ChPT in the Baryon Superfluid Phase

The ground-state configuration $\langle U \rangle = E^T$ corresponding to the hadronic phase is indeed realized as a stationary point of the effective potential $V_{\mathrm{ChPT}}^{\mathcal{O}(p^2)} \equiv -\left\langle \mathcal{L}_{\mathrm{ChPT}}^{\mathcal{O}(p^2)} \right\rangle$, unless the

chemical potential is sufficiently large (or $j \neq 0$). On the other hand, this configuration is altered for $\mu_q > m_\pi^{(H)}/2$ due to the emergence of diquark condensates, resulting in the baryon superfluid phase. This phase transition is also signaled by the diquark mass; when $\mu_q > m_\pi^{(H)}/2$, the diquark mass turns to negative, as seen from Equation (97). In this subsection, we explain how the ChPT Lagrangian is modified in the superfluid phase.

In the baryon superfluid phase, the VEV of $\langle U \rangle$ is rotated from E^T to

$$U_\alpha \equiv V_\alpha E^T V_\alpha^T = V_\alpha^2 E^T \quad \text{with} \quad V_\alpha^2 = e^{i\alpha \bar{X}} . \tag{98}$$

Here, following Refs. [39,40], we employ $\bar{X} = -2\sqrt{2}X^5$ as the rotation axis in such a way that Equation (98) at a sufficiently large μ_q approaches $U_d \equiv \text{diag}(\tau_f^2, \tau_f^2)$ and the diquark condensates dominate over the ground state. Thus, deviation from $\alpha = 0$ denotes the beginning of the chiral restoration and emergence of superfluidity. In association with the rotation of the ground-state configuration (98), it is useful to rotate subgroup H so as to keep parametrizing π^a as the representative of G/H appropriately. When we define the rotated generators

$$S_\alpha^i = V_\alpha S^i V_\alpha^\dagger \quad , \quad X_\alpha^a = V_\alpha X^a V_\alpha^\dagger , \tag{99}$$

one can easily show that they satisfy the following algebras of $\mathcal{H}$ and $\mathcal{G} - \mathcal{H}$ correctly,

$$S_\alpha^i U_\alpha = -U_\alpha (S^i)^T \quad , \quad X^a U_\alpha = U_\alpha (X^a)^T , \tag{100}$$

similarly to Equations (18) and (19). Thus, adopting these generators, the representative of rotated-G/H is provided by

$$\xi_\alpha \equiv e^{i\pi^a X_\alpha^a} = V_\alpha \xi V_\alpha^\dagger \quad \left(\xi_\alpha \xrightarrow{G} g\xi_\alpha h_\alpha^\dagger \quad \text{with} \quad h_\alpha \in H \right) , \tag{101}$$

with ξ being Equation (74). Similarly, the other important building block in constructing the ChPT Lagrangian is provided by

$$\tilde{\xi}_\alpha \equiv U_\alpha \xi_\alpha^* U_\alpha^\dagger \quad \left(\tilde{\xi}_\alpha \xrightarrow{G} U_\alpha g^* U_\alpha^\dagger \tilde{\xi}_\alpha h_\alpha^\dagger \right) , \tag{102}$$

like Equation (78). With these quantities, following the same procedure as in Section 3.1, one can finally arrive at (the rotated field $\hat{\zeta}_\alpha$ would be given by $\hat{\zeta}_\alpha = B_0 \xi_\alpha^\dagger \zeta \Sigma_\alpha \xi_\alpha$, the G-transformation low of which is $\zeta_\alpha \to h_\alpha \zeta_\alpha h_\alpha^\dagger$)

$$\mathcal{L}_{\text{ChPT}}^{\mathcal{O}(p^2)} = \frac{f_0^2}{4} \text{tr}[D_\mu U_\alpha^\dagger D^\mu U_\alpha] + \text{tr}[U_\alpha \zeta_\alpha^\dagger + U_\alpha^\dagger \zeta_\alpha] . \tag{103}$$

We note that the structure of G is not modified even in the superfluid phase, whereas subgroup H is rotated, and thus the covariant derivative associated with the gauge symmetry of G takes the same form as Equation (90).

The value of angle α fixing the ground-state configuration is determined by a stationary condition of the potential within the mean-field approximation:

$$V_{\text{ChPT}}^{\mathcal{O}(p^2)} \equiv -\left\langle \mathcal{L}_{\text{ChPT}}^{\mathcal{O}(p^2)} \right\rangle = 2f_0^2 \left[\mu_q^2(1 - \cos 2\alpha) + \left(m_\pi^{(H)} \right)^2 \cos \alpha \right] , \tag{104}$$

namely,

$$2\mu_q^2 \sin 2\alpha = \left(m_\pi^{(H)} \right)^2 \sin \alpha , \tag{105}$$

which yields ($\mu_{\mathrm{cr}} \equiv m_\pi^{(\mathrm{H})}/2$)

- for $\mu_q < \mu_{\mathrm{cr}}: \alpha = 0$,

- for $\mu_{\mathrm{cr}} \le \mu_q: \cos\alpha = \dfrac{\left(m_\pi^{(\mathrm{H})}\right)^2}{4\mu_q^2}$. (106)

The former and latter solutions represent the hadronic and baryon superfluid phases, respectively. Upon this ground state, the ChPT Lagrangian is expanded to be

$$
\begin{aligned}
\mathcal{L}_{\mathrm{ChPT}}^{\mathcal{O}(p^2)} &= \frac{1}{2}\partial_\mu \pi^a \partial^\mu \pi^a + 2\mu_q \cos\alpha\,(\partial_0 \pi^4 \pi^5 - \pi^4 \partial_0 \pi^5) \\
&\quad - \sum_{a=1,2,3} \frac{m_\pi^2}{2}\pi^a \pi^a - \frac{m_4^2}{2}\pi^4 \pi^4 - \frac{m_5^2}{2}\pi^5 \pi^5 + \cdots ,
\end{aligned}
$$
(107)

in which we have defined

$$
\begin{aligned}
m_\pi^2 &= \left(m_\pi^{(\mathrm{H})}\right)^2 \cos\alpha - 2\mu_q^2(\cos 2\alpha - 1) = 4\mu_q^2 , \\
m_4^2 &= \left(m_\pi^{(\mathrm{H})}\right)^2 \cos\alpha - 2\mu_q^2(\cos 2\alpha + 1) = 0 , \\
m_5^2 &= \left(m_\pi^{(\mathrm{H})}\right)^2 \cos\alpha - 4\mu_q^2 \cos 2\alpha = 4\mu_q^2 - \frac{\left(m_\pi^{(\mathrm{H})}\right)^4}{4\mu_q^2} .
\end{aligned}
$$
(108)

Therefore, the pion mass is found to be simply given by $2\mu_q$ in the superfluid phase. In this phase, the $U(1)$ baryon-number violation leads to a rotated kinetic mixing with $\cos\alpha$ accompanied for diquark and antidiquark states, as shown in the second term in Equation (107).

Based on the derived mass formulas of pions and (anti)diquarks, we can depict μ_q dependences of the masses predicted by the $\mathcal{O}(p^2)$ ChPT with a vanishing diquark source, shown in the left panel of Figure 3. In the hadronic phase, the hadron masses exhibit stable μ_q dependences, as analytically evaluated in Equations (96) and (97). In the baryon superfluid phase, in addition to the monotonic pion mass increment with formula (108), the diquark mass is found to be always zero, indicating that this state is responsible for the NG boson associated with the breakdown of $U(1)$ baryon-number symmetry [39,40].
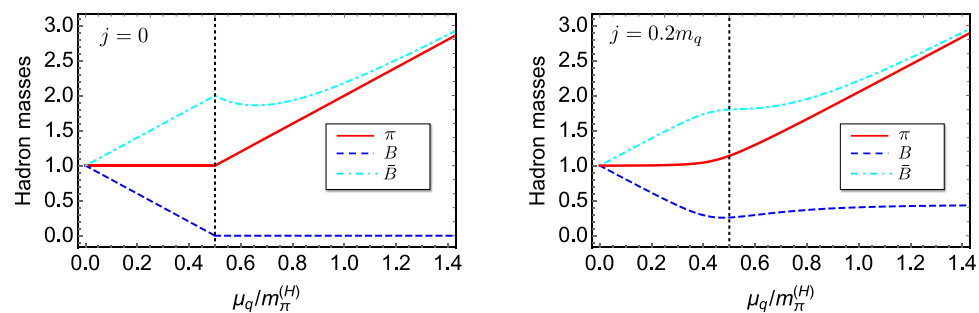
Figure 3. μ_q dependences of the hadron masses evaluated by the $\mathcal{O}(p^2)$ ChPT with $j = 0$ (**left**) and $j = 0.2m_q$ (**right**).

3.4. ChPT with a Diquark Source j

In order to achieve the baryon superfluid phase appropriately on the lattice, it is necessary to incorporate a diquark source j; then, we take, or extrapolate, the $j \to 0$ limit at its end. Sometimes, this extrapolation is not easily achieved, and the diquark source effects remain in the actual lattice simulation. Then, in order to gain insights into the source effect based on effective models, here, we keep j finite.

As demonstrated in Section 2.3, the diquark source j is introduced by replacing the spin-0 spurion field as $p^5 \to \langle p^5 \rangle = j$. Proceeding with this treatment within the ChPT framework, as gathered from Equation (103), the phase of the bare-mass term is modified as $\cos \alpha \to \cos(\alpha - \phi)$ with $\tan \phi = j/m_q$. Hence, in the presence of j, the phase α is not simply fixed by Equation (106), but is determined by the following modified stationary condition:

$$2\mu_q^2 \sin 2\alpha = \left(m_\pi^{(\mathrm{H})} \right)^2 \sin(\alpha - \phi) . \tag{109}$$

This equation implies that α is nonzero when $j \neq 0$ even in the vacuum ($\mu_q = 0$); that is, the superfluidity always governs the system due to the explicit $U(1)_B$ symmetry breaking.

With a finite j, the NG boson masses read

$$
\begin{aligned}
m_\pi^2 &= \bar{m}_\pi^2 \cos(\alpha - \phi) - 2\mu_q^2 (\cos 2\alpha - 1) = \frac{\cos \phi}{\cos \alpha} \bar{m}_\pi^2 , \\
m_4^2 &= \bar{m}_\pi^2 \cos(\alpha - \phi) - 2\mu_q^2 (\cos 2\alpha + 1) = \frac{\sin \phi}{\sin \alpha} \bar{m}_\pi^2 , \\
m_5^2 &= \bar{m}_\pi^2 \cos(\alpha - \phi) - 4\mu_q^2 \cos 2\alpha = \left(\frac{\cos^2 \alpha}{\sin \alpha} \sin \phi + \frac{\sin^2 \alpha}{\cos \alpha} \cos \phi \right) \bar{m}_\pi^2 ,
\end{aligned}
\tag{110}
$$

where $\bar{m}_\pi^2 \equiv 2B_0 \sqrt{m_q^2 + j^2}$ is the vacuum pion mass. In these equations, we made use of the corrected stationary condition (109) to find the right-most expressions. When we take $j = 0.2 m_q$ as a demonstration, the hadron mass spectra at finite μ_q are obtained, as depicted in the right panel of Figure 3, where μ_q dependences are slightly modified. In particular, the NG mode disappears, reflecting the explicit $U(1)_B$ symmetry violation.

From the matching (30), the chiral and diquark condensates can be evaluated within the ChPT as

$$
\begin{aligned}
\langle \bar{\psi}\psi \rangle &= \left. \frac{\partial \mathcal{L}_{\mathrm{ChPT}}^{\mathcal{O}(p^2)}}{-\partial s^0} \right|_{\langle \zeta \rangle, \langle \zeta_\mu \rangle} = -4G f_0^2 \cos \alpha , \\
\langle \psi\psi \rangle &= \left. \frac{\partial \mathcal{L}_{\mathrm{ChPT}}^{\mathcal{O}(p^2)}}{-\partial p^0} \right|_{\langle \zeta \rangle, \langle \zeta_\mu \rangle} = -4G f_0^2 \sin \alpha ,
\end{aligned}
\tag{111}
$$

respectively. This expression is universal to any value of μ_q.

The broken current within the ChPT is evaluated by taking a derivative of $\mathcal{L}_{\mathrm{ChPT}}^{\mathcal{O}(p^2)}$ with respect to $\zeta_X^{\mu a} \equiv -2\sqrt{2} V_\mu'^a$ and setting Equation (26), resulting in

$$
\begin{aligned}
j_{X\mu}^a &= -f_0 \cos \alpha \, \partial_\mu \pi^a + \cdots \quad (\text{for } a = 1 - 3) , \\
j_{X\mu}^4 &= -f_0 \cos \alpha \partial_\mu \pi^4 - 2f_0 \mu_q \delta_{\mu 0} \cos 2\alpha \, \pi^5 + \cdots \quad (\text{for } a = 4) , \\
j_{X\mu}^5 &= -f_0 \partial_\mu \pi^5 + 2f_0 \mu_q \delta_{\mu 0} \cos \alpha \, \pi^4 + \cdots \quad (\text{for } a = 5) .
\end{aligned}
\tag{112}
$$

Similarly the $U(1)_B$ current is calculated to be

$$j_{B\mu} = -2\sqrt{2} f_\pi \sin \alpha \partial_\mu \pi^4 - 4\sqrt{2} f_\pi \mu_q \delta_{\mu 0} \sin 2\alpha \, \pi^5 + \cdots , \tag{113}$$

by taking a derivative with respect to $\zeta_B^\mu \equiv V^{\mu, i=4}$. From the pionic sector in Equation (112), one can easily see

$$f_\pi = f_0 \cos \alpha \tag{114}$$

at any μ_q, from the argument in Section 2.5. Thus, utilizing the pion mass formula in Equation (110) together with the chiral condensate (111), the GOR relation (66) is readily confirmed.

As for the baryonic sector, when taking $\mu_q = 0$ so as to eliminate difficulties due to the mixings, the decay constants associated with the baryonic broken current and $U(1)_B$ current read

$$f_5 \;=\; f_0 \quad (a = 5)\,, \tag{115}$$

and

$$f_B = 2\sqrt{2} f_\pi \sin\alpha\,, \tag{116}$$

respectively. Thus, using mass formulas (110) and decay constants (115) and (116), we can easily verify that GOR relations (67) and (68) certainly hold within the ChPT. (It seems that $\left(\frac{f_B}{2\sqrt{2}}\right)^2 m_4^2 = -\frac{\langle\bar\psi\psi\rangle}{2}$ holds at any μ_q.)

3.5. Thermodynamic Properties

The ChPT Lagrangian in the hadronic and superfluid phases was derived in Section 3.2 and Section 3.3, respectively, and thus we are now ready to evaluate thermodynamic properties such as pressure, energy density, and sound velocity. Here, we exhibit μ_q dependences of those quantities with a vanishing j [10,77].

From Lagrangians (89) and (103), the pressure $p = \langle\mathcal{L}\rangle$ in the hadronic and superfluid phases is evaluated to be

$$
\begin{aligned}
p_{\text{ChPT}}^{(\text{H})} &= 2f_0^2\big(m_\pi^{(\text{H})}\big)^2\,,\\
p_{\text{ChPT}}^{(\text{BS})} &= f_0^2\big(m_\pi^{(\text{H})}\big)^2\left(\bar\mu^2 + \frac{1}{\bar\mu^2}\right),
\end{aligned}
\tag{117}
$$

respectively, where $\bar\mu = \mu_q/\mu_{\text{cr}} = 2\mu_q/m_\pi^{(\text{H})}$. The stability of the vacuum ($\mu_q = 0$) requires that the vacuum pressure be zero, and thus the correct pressure in the superfluid phase is the following subtracted one:

$$p_{\text{ChPT}}^{\text{sub}} \equiv p_{\text{ChPT}}^{(\text{BS})} - p_{\text{ChPT}}^{(\text{H})} = f_0^2\big(m_\pi^{(\text{H})}\big)^2\left(\bar\mu - \frac{1}{\bar\mu}\right)^2. \tag{118}$$

With this subtracted pressure, the baryon-number density and baryon susceptibility are derived to be

$$
\begin{aligned}
n_{\text{ChPT}} &= \frac{\partial p_{\text{ChPT}}^{\text{sub}}}{\partial \mu_q} = \frac{2f_0^2\big(m_\pi^{(\text{H})}\big)^2}{\mu_q}\left(\bar\mu^2 - \frac{1}{\bar\mu^2}\right),\\
\chi_{\text{ChPT}} &= \frac{\partial^2 p_{\text{ChPT}}^{\text{sub}}}{\partial \mu_q^2} = 8f_0^2\left(1 + \frac{3}{\bar\mu^4}\right),
\end{aligned}
\tag{119}
$$

respectively. Moreover, the (subtracted) energy density is also straightforwardly evaluated as

$$\epsilon_{\text{ChPT}}^{\text{sub}} = -p_{\text{ChPT}}^{\text{sub}} + \mu_q n_{\text{ChPT}} = f_0^2\big(m_\pi^{(\text{H})}\big)^2 \frac{(\bar\mu^2 + 3)(\bar\mu^2 - 1)}{\bar\mu^2}\,. \tag{120}$$

Another significant quantity which characterizes a dense matter is the (squared) sound velocity $c_s^2 = \partial p / \partial \epsilon$ defined along the isentropic trajectory. As long as we stick to zero temperature, the trajectory is identical to the $T = 0$ line and the sound velocity is simply evaluated using

$$c_s^2 = \frac{n}{\mu_q \chi} . \tag{121}$$

Hence, from Equation (119), one can find

$$\left(c_s^{\text{ChPT}}\right)^2 = \frac{n_{\text{ChPT}}}{\mu_q \chi_{\text{ChPT}}} = \frac{1 - 1/\bar{\mu}^4}{1 + 3/\bar{\mu}^4} . \tag{122}$$

This formula will be used in Section 4.6 to see a difference between the ChPT and LSM results, focusing on the bulk structure of dense QC_2D.

3.6. Hidden Local Symmetry

The ChPT is capable of describing NG boson dynamics based on a systematic low-energy expansion since the theory is constructed upon the Maurer–Cartan 1-form (76) including a derivative. However, the expansion cannot converge as the energy scale is increased due to the appearance of other hadronic modes. Among them, spin-1 hadrons such as ρ mesons and axialvector diquarks can also be treated in the systematic-expansion scheme as an extension of the ChPT, by regarding them as gauge bosons associated with subgroup H. This systematic treatment of the spin-1 hadrons is called the *hidden local symmetry (HLS) technique* [78]. In this subsection, we briefly review how the HLS extension is achieved in the ChPT of QC_2D. For a detailed argument, please see Ref. [52].

In the decomposition of $\Sigma = \xi E^T \xi^T$, one can find redundant degrees of freedom, σ^i, incorporated via

$$\xi = \xi(\pi)\xi(\sigma) \quad \text{with} \quad \xi(\pi) = e^{i\pi^a X^a / f_\pi} \quad \text{and} \quad \xi(\sigma) = e^{i\sigma^i S^i / f_\sigma} , \tag{123}$$

which is hidden in Σ because of Equation (18). These secret fields can be identified as NG bosons of the spontaneous breakdown of $H_{\text{local}} = [Sp(4)]_{\text{local}}$. In other words, now, the whole symmetry is extended from $SU(4)$ to $SU(4) \times [Sp(4)]_{\text{local}}$, and $\xi(\pi)$ and $\xi(\sigma)$ transform as

$$\xi(\pi) \to g\xi(\pi)h^\dagger(x) , \quad \xi(\sigma) \to h(x)\xi(\sigma)h^\dagger(x) , \tag{124}$$

respectively. Accordingly, the gauge bosons associated with $H_{\text{local}} = [Sp(4)]_{\text{local}}$, V_μ, which transform as

$$V_\mu \to h(x)V_\mu h^\dagger(x) - i\partial_\mu h(x)h^\dagger(x) , \tag{125}$$

join the low-energy spectrum. This V_μ belongs to the algebra of $\mathcal{H}$ containing 10 degrees of freedom: $V_\mu = V_\mu^i S^i$. They correspond to three ρ mesons, one ω meson, three axialvector diquark baryons, and three axialvector antidiquark baryons.

With transformation laws (124), we only need to change $h(g, \pi)$ to $h(x)$ in Formulas (75) and (83). Therefore, when we define

$$\hat{\alpha}_{\perp,\mu} \equiv \frac{1}{2i}(\mathcal{D}_\mu \xi^\dagger \xi - \mathcal{D}_\mu \tilde{\xi}^\dagger \tilde{\xi}) ,$$

$$\hat{\alpha}_{\parallel,\mu} \equiv \frac{1}{2i}(\mathcal{D}_\mu \xi^\dagger \xi + \mathcal{D}_\mu \tilde{\xi}^\dagger \tilde{\xi}) , \tag{126}$$

as extensions of Equation (88) with the covariant derivatives

$$
\begin{aligned}
\mathcal{D}_\mu \xi^\dagger &= \partial_\mu \xi^\dagger - iV_\mu \xi^\dagger + i\xi^\dagger \zeta_\mu \,, \\
\mathcal{D}_\mu \tilde{\xi}^\dagger &\equiv \partial_\mu \tilde{\xi}^\dagger - iV_\mu \tilde{\xi}^\dagger - i\tilde{\xi}^\dagger E^T \zeta_\mu^T E \,,
\end{aligned}
\tag{127}
$$

one can easily check

$$
\hat{\alpha}_{\perp,\mu} \to h(x)\hat{\alpha}_{\perp,\mu}h^\dagger(x) \,, \quad \hat{\alpha}_{\parallel,\mu} \to h(x)\hat{\alpha}_{\parallel,\mu}h^\dagger(x) \,,
\tag{128}
$$

and the HLS Lagrangian is readily constructed as

$$
\mathcal{L}_{\mathrm{HLS}}^{\mathcal{O}(p^2)} = -\frac{1}{2g_\rho^2}\mathrm{tr}[V_{\mu\nu}V^{\mu\nu}] + f_\pi^2\mathrm{tr}[\hat{\alpha}_{\perp,\mu}\hat{\alpha}_\perp^\mu] + f_\sigma^2\mathrm{tr}[\hat{\alpha}_{\parallel,\mu}\hat{\alpha}_\parallel^\mu] + f_\pi^2\mathrm{tr}[\hat{\zeta} + \hat{\zeta}^\dagger] \,.
\tag{129}
$$

In this Lagrangian, the (dressed) spurion field transforms as $\hat{\zeta} \to h(x)\hat{\zeta}h^\dagger(x)$, and we incorporate the kinetic term of the vector bosons from their field strength

$$
V_{\mu\nu} = \partial_\mu V_\nu - \partial_\nu V_\mu - i[V_\mu, V_\nu] \,,
\tag{130}
$$

with an HLS-gauge coupling g_ρ. Within the unitary gauge, the NG bosons are simply absorbed by the longitudinal modes of the vector bosons, leading to $\sigma^i = 0$.

The HLS Lagrangian (129) only includes $\mathcal{O}(p^2)$ contributions. The $\mathcal{O}(p^4)$ terms are listed in Ref. [52] and their contributions to spin-1 hadron masses at finite μ_q are also explored in the literature.

4. Linear Sigma Model

The ChPT which describes five NG bosons—three pions, a diquark, and an antidiquark—is reviewed in Section 3, as the low-energy effective model of QC$_2$D. One way to extend the model to incorporate spin-1 bosons systematically based on the HLS technique is also briefly explained in Section 3.6. Although those frameworks are powerful thanks to their systematic expansion with the power counting, we know that QC$_2$D involves other light excitations, e.g., the scalar mesons and negative-parity diquark baryons that cannot be treated by those models. Lattice simulations have been, indeed, used to measure those hadrons. In particular, the recent lattice simulation claims that in the superfluid phase, there exists an iso-singlet 0^- mode as the second-lightest hadron, which is lighter than the pions [41]. This fact implies that the ChPT is no longer a correct low-energy effective model of dense QC$_2$D, so it is inevitable to construct another effective model which is capable of describing such hadrons as well based on the Pauli–Gürsey $SU(4)$ symmetry. Thus, in this section, we introduce the LSM pursuant to the linear representation of the $SU(4)$ symmetry treating $0^\pm$ mesons and diquark baryons comprehensively.

4.1. Model Construction

In Equation (91), the following 4×4-matrix bilinear operator made of Ψ,

$$
\Phi_{ij} = \Psi_j^T \sigma^2 \tau_c^2 \Psi_i \,,
\tag{131}
$$

is introduced to understand the bilinear representation of NG boson π^as, which are incorporated nonlinearly within the ChPT framework. Meanwhile, the bilinear operator Φ contains 12 degrees of freedom as real numbers since $\Phi = -\Phi^T$, implying that we

can assign 12 hadronic states to parametrize Φ maximumly when employing the linear representation of Pauli–Gürsey $SU(4)$ symmetry. Thus, the following 12 hadron fields,

$$\eta \sim \bar{\psi} i \gamma_5 \psi \,, \quad \pi^\pm \sim \frac{1}{\sqrt{2}} \bar{\psi} i \gamma_5 \tau_f^\mp \psi \,, \quad \pi^0 \sim \bar{\psi} i \gamma_5 \tau_f^3 \psi \,, \quad \sigma \sim \bar{\psi}\psi \,, \quad a_0^\pm \sim \frac{1}{\sqrt{2}} \bar{\psi} \tau_f^\mp \psi \,,$$

$$a_0^0 \sim \bar{\psi} \tau_f^3 \psi \,, \quad B \sim -\frac{i}{\sqrt{2}} \psi^T C \gamma_5 \tau^2 \tau_f^2 \psi \,, \quad \bar{B} \sim -\frac{i}{\sqrt{2}} \psi^\dagger C \gamma_5 \tau^2 \tau_f^2 \psi^* \,,$$

$$B' \sim -\frac{1}{\sqrt{2}} \psi^T C \tau^2 \tau_f^2 \psi \,, \quad \bar{B}' \sim \frac{1}{\sqrt{2}} \psi^\dagger C \tau^2 \tau_f^2 \psi^* \,, \tag{132}$$

can be embedded into Φ as

$$\Phi \sim \Sigma \equiv \frac{1}{2} \begin{pmatrix} 0 & -B' + iB & \frac{\sigma - i\eta + a_0^0 - i\pi^0}{\sqrt{2}} & a_0^+ - i\pi^+ \\ B' - iB & 0 & a_0^- - i\pi^- & \frac{\sigma - i\eta - a_0^0 + i\pi^0}{\sqrt{2}} \\ -\frac{\sigma - i\eta + a_0^0 - i\pi^0}{\sqrt{2}} & -a_0^- + i\pi^- & 0 & -\bar{B}' + i\bar{B} \\ -a_0^+ + i\pi^+ & -\frac{\sigma - i\eta - a_0^0 + i\pi^0}{\sqrt{2}} & \bar{B}' - i\bar{B} & 0 \end{pmatrix}. \tag{133}$$

In this equation, Σ is defined as a mass-dimension $+1$ matrix with a normalization factor of $1/2$, chosen for later convenience. Matrix (133) is expressed concisely in terms of the generator X^a together with the symplectic matrix E as

$$\Sigma = (\mathcal{S}^a - i\mathcal{P}^a) X^a E \,, \tag{134}$$

where the $\mathcal{S}^a$s and $\mathcal{P}^a$s ($a = 0\text{–}5$) are related to the hadron fields by

$$\eta = \mathcal{P}^0 \,, \quad \pi^\pm = \frac{\mathcal{P}^1 \mp i\mathcal{P}^2}{\sqrt{2}} \,, \quad \pi^0 = \mathcal{P}^3 \,, \quad B = \frac{\mathcal{P}^5 - i\mathcal{P}^4}{\sqrt{2}} \,, \quad \bar{B} = \frac{\mathcal{P}^5 + i\mathcal{P}^4}{\sqrt{2}} \,,$$

$$\sigma = \mathcal{S}^0 \,, \quad a_0^\pm = \frac{\mathcal{S}^1 \mp i\mathcal{S}^2}{\sqrt{2}} \,, \quad a_0^0 = \mathcal{S}^3 \,, \quad B' = \frac{\mathcal{S}^5 - i\mathcal{S}^4}{\sqrt{2}} \,, \quad \bar{B}' = \frac{\mathcal{S}^5 + i\mathcal{S}^4}{\sqrt{2}} \,. \tag{135}$$

Quantum numbers of these spin-0 hadrons are tabulated in Table 1.

Table 1. Quantum numbers of the hadrons in Equation (135).

Hadron	Spin and Parity (J^P)	Quark Number	Isospin
η	0^-	0	0
π	0^-	0	1
σ	0^+	0	0
a_0	0^+	0	1
$B\ (\bar{B})$	0^+	$+2\ (-2)$	0
$B'\ (\bar{B}')$	0^-	$+2\ (-2)$	0

From interpolating field (131), the $SU(4)$ transformation law of Σ is readily understood to be

$$\Sigma \to g \Sigma g^T \quad \text{with} \quad g \in SU(4) \,. \tag{136}$$

Thus, one can construct an LSM Lagrangian preserving the $SU(4)$ symmetry as [44]

$$\begin{aligned} \mathcal{L}_{\text{LSM}} &= \text{tr}[D_\mu \Sigma^\dagger D^\mu \Sigma] - m_0^2 \text{tr}[\Sigma^\dagger \Sigma] - \lambda_1 \left(\text{tr}[\Sigma^\dagger \Sigma]\right)^2 - \lambda_2 \text{tr}[(\Sigma^\dagger \Sigma)^2] \\ &\quad + \bar{c}\, \text{tr}[\zeta^\dagger \Sigma + \Sigma^\dagger \zeta] + \mathcal{L}_{\text{anom.}} \,, \end{aligned} \tag{137}$$

where $\mathcal{L}_{\text{anom.}}$ is responsible for the $U(1)_A$ anomaly of QC$_2$D, which generally takes the form of

$$\mathcal{L}_{\text{anom.}} = \frac{a}{2}\text{tr}[\tilde{\Sigma}\Sigma + \tilde{\Sigma}^\dagger\Sigma^\dagger] + \frac{c_1}{4}\left(\text{tr}[\tilde{\Sigma}\Sigma + \tilde{\Sigma}^\dagger\Sigma^\dagger]\right)^2 + \frac{c_2}{2}\text{tr}[\Sigma^\dagger\Sigma]\text{tr}[\tilde{\Sigma}\Sigma + \tilde{\Sigma}^\dagger\Sigma^\dagger] , \quad (138)$$

with $\tilde{\Sigma}_{ij} = \frac{1}{2}\epsilon_{ijkl}\Sigma_{kl}$. These terms indeed break $U(1)_A$ symmetry, with which the $U(1)_A$ transformation of Σ is simply generated by $\Sigma \to \text{e}^{-i\theta_A}\Sigma\text{e}^{-i\theta_A} = \text{e}^{-2i\theta_A}\Sigma$. In Equation (137), the covariant derivative is defined by

$$D_\mu\Sigma = \partial_\mu\Sigma - i\zeta_\mu\Sigma - i\Sigma\zeta_\mu^T , \quad (139)$$

and the spurion fields ζ and ζ_μ exhibit transformation laws of

$$\zeta \to g\zeta g^T, \quad \zeta_\mu \to g\zeta_\mu g^\dagger - i\partial_\mu gg^\dagger , \quad (140)$$

which are, of course, the same as the ones introduced in the QC$_2$D Lagrangian in Equation (21). In the end, we replace them with the VEVs in Equation (26) using Equation (24) to take into account the quark mass, diquark source, and chemical potential effects. We note that the $\det\Sigma + \det\Sigma^\dagger$ term for the anomaly effects adopted in Ref. [44] is obtained from the c_1 term with the help of the following identity:

$$\left(\text{tr}[\tilde{\Sigma}\Sigma + \tilde{\Sigma}^\dagger\Sigma^\dagger]\right)^2 = -8\text{tr}[(\Sigma^\dagger\Sigma)^2] + 4\left(\text{tr}[\Sigma^\dagger\Sigma]\right)^2 + 16(\det\Sigma + \det\Sigma^\dagger) . \quad (141)$$

The latest lattice result where disconnected diagrams are also included seems to imply that $m_\eta^{(\text{H})}/m_\pi^{(\text{H})}$ is close to unity, and the $U(1)_A$ anomaly effects may be suppressed, at least in the vacuum [79]. Hence, in the following arguments, we will ignore the anomalous contributions, $a = c_1 = c_2 = 0$, otherwise stated.

4.2. Phase Structure from the LSM

As in the ChPT analysis, the current LSM undergoes a phase transition to the baryon superfluid phase, driven by the emergence of diquark condensates. Unlike the ChPT, within the LSM based on linear representation, such effects can be represented directly by a mean field of the positive-parity diquark baryon. Hence, here, we consider

$$\sigma_0 \equiv \langle\sigma\rangle , \quad \Delta \equiv \langle\mathcal{P}^5\rangle , \quad (142)$$

for the chiral condensate and diquark condensate. From formula (30) matching the underlying QC$_2$D, diquark condensates within the LSM are evaluated to be

$$\begin{aligned} \langle\bar{\psi}\psi\rangle &= \left.\frac{\partial\mathcal{L}_{\text{LSM}}}{-\partial s^0}\right|_{\langle\zeta\rangle,\langle\zeta_\mu\rangle} = -\sqrt{2}\bar{c}\sigma_0 , \\ \langle\psi\psi\rangle &= \left.\frac{\partial\mathcal{L}_{\text{LSM}}}{-\partial p^0}\right|_{\langle\zeta\rangle,\langle\zeta_\mu\rangle} = -\sqrt{2}\bar{c}\Delta . \end{aligned} \quad (143)$$

At the mean-field level, the effective potential takes the form of

$$V_{\text{LSM}}^{\text{eff}} = -2\mu_q^2\Delta^2 + \frac{m_0^2}{2}(\Delta^2 + \sigma_0^2) + \frac{\tilde{\lambda}}{4}(\sigma_0^2 + \Delta^2)^2 - \sqrt{2}\bar{c}(m_q\sigma_0 + j\Delta) , \quad (144)$$

where $\tilde{\lambda} = (4\lambda_1 + \lambda_2)/4$. The phase structures, i.e., μ_q dependences of σ_0 and Δ, are determined by finding stationary points of this potential with respect to these mean fields,

$$\left(m_\pi^2 - \frac{\sqrt{2}\bar{c}m_q}{\sigma_0}\right)\sigma_0 = 0 \,, \quad \left(m_\pi^2 - 4\mu_q^2 - \frac{\sqrt{2}\bar{c}j}{\Delta}\right)\Delta = 0 \,, \tag{145}$$

from which the pion mass at any μ_q reads

$$m_\pi^2 = m_0^2 + \tilde{\lambda}(\sigma_0^2 + \Delta^2) \tag{146}$$

by expanding Lagrangian (137) upon σ_0 and Δ. Here, we take $j = 0$ to exclude the diquark condensates in the vacuum. In this case, solving the gap equations yields

- $$\text{for} \quad \mu_q < \mu_{cr}: \quad \sigma_0 = \sigma_0^{(H)} = (\text{constant}) \,, \quad \Delta = 0 \,.$$

- $$\text{for} \quad \mu_{cr} \le \mu_q: \quad \sigma_0 = \frac{m_q\bar{c}}{2\sqrt{2}}\mu_q^{-2} \,, \quad \Delta = \left[(\sigma_0^{(H)})^2 - \sigma_0^2 + \frac{1}{\tilde{\lambda}}\left(4\mu_q^2 - (m_\pi^{(H)})^2\right)\right]^{1/2} \,,$$
$$\tag{147}$$

where $m_\pi^{(H)} = \sqrt{2}m_q\bar{c}/\sigma_0^{(H)}$ is the pion mass in the hadronic phase. Thus, the critical chemical potential $\mu_{cr} = m_\pi^{(H)}/2$ separating the hadronic and baryon superfluid phases is identical to that found in the ChPT framework. It should be noted that the NJL model analysis also derives the same μ_{cr} [47].

The μ_q dependences of σ_0 and Δ with $j = 0$, $j = 0.2m_q$, and $j = 0.5m_q$ are depicted in Figure 4. In plotting this figure, we used large-N_c suppression [80] for the parameters, i.e., $\lambda_1 = 0$, and adopted

$$m_\pi^{(H)} = 738\,\text{MeV} \,, \quad m_{B'(\bar{B}')}^{(H)} = 1611\,\text{MeV} \,, \tag{148}$$

as inputs from the measured hadron masses on the lattice [41]. In addition,

$$\sigma_0^{(H)} = 250\,\text{MeV} \tag{149}$$

was employed as a typical value for the chiral condensate in order to fix the remaining parameter. The figure indicates that when j is finite, Δ always acquires nonzero values leading to the superfluid phase, whereas the hadronic and superfluid phases are well separated for $j = 0$, as analytically found in Equation (147). As long as j is not sufficiently large, the prominent chiral restoration and evolution of Δ start at $\mu_q \approx m_\pi^{(H)}/2$.
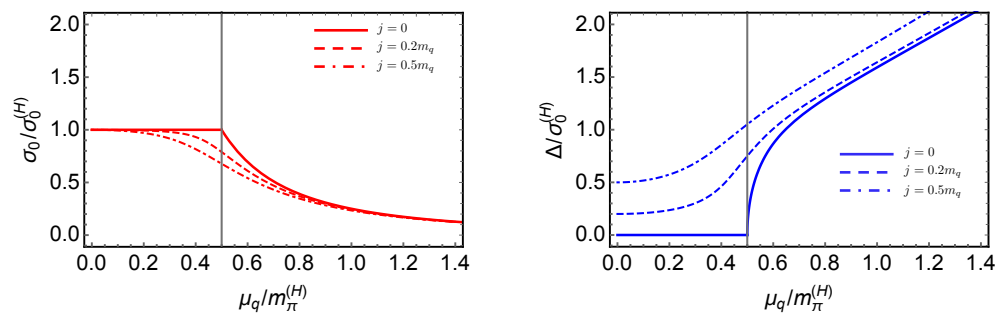
Figure 4. μ_q dependences of the mean fields σ_0 and Δ with $j = 0$ (solid), $j = 0.2m_q$ (dashed), and $j = 0.5m_q$ (dot–dashed). The vertical gray line represents $\mu_q/m_\pi^{(H)} = 1/2$.

4.3. Hadron Mass Spectrum at Finite μ_q

In this subsection, we restrict ourselves to a vanishing diquark source, $j = 0$. In this limit, the parameters are fixed to be

$$\lambda_1 = 0 , \quad \lambda_2 = 65.6 , \quad m_0^2 = -(693 \, \text{MeV})^2 , \quad m_q \bar{c} = (456 \, \text{MeV})^3 , \tag{150}$$

where $\lambda_1 = 0$ stems from the large-N_c expansion [80]. With these parameters, we are ready to numerically explore the hadron masses in cold and dense QC$_2$D matter with the LSM. The pion mass formula is provided in Equation (146). The other hadron masses are evaluated by reading off the quadratic terms of each field in Equation (137), which reads

$$m_{a_0}^2 = m_\pi^2 + \frac{\lambda_2}{2}(\sigma_0^2 + \Delta^2) , \quad m_{\mathcal{P}^4}^2 = m_\pi^2 - 4\mu_q^2 , \quad m_{\mathcal{P}^5}^2 = m_\pi^2 - 4\mu_q^2 + 2\tilde{\lambda}\Delta^2 ,$$
$$m_\sigma^2 = m_\pi^2 + 2\tilde{\lambda}\sigma_0^2 , \quad m_{\mathcal{P}^5\sigma}^2 = 2\tilde{\lambda}\sigma_0\Delta , \tag{151}$$

$$m_{\mathcal{S}^4}^2 = m_\pi^2 - 4\mu_q^2 + \frac{\lambda_2}{2}(\sigma_0^2 + \Delta^2) , \quad m_{\mathcal{S}^5}^2 = m_\pi^2 - 4\mu_q^2 + \frac{\lambda_2}{2}\sigma_0^2 ,$$
$$m_\eta^2 = m_\pi^2 + \frac{\lambda_2}{2}\Delta^2 , \quad m_{\mathcal{S}^5\eta}^2 = \frac{\lambda_2}{2}\sigma_0\Delta . \tag{152}$$

We note that $(\mathcal{P}^4, \mathcal{P}^5, \sigma)$ and $(\mathcal{S}^4, \mathcal{S}^5, \eta)$ exhibit state mixings due to the baryon-number violation, leading to the following 3×3 propagator-inverse matrices in the momentum space:

$$iD_{\mathcal{P}^4\mathcal{P}^5\sigma}^{-1}(p) = \begin{pmatrix} p^2 - m_{\mathcal{P}^4}^2 & 2i\mu_q p_0 & 0 \\ -2i\mu_q p_0 & p^2 - m_{\mathcal{P}^5}^2 & -m_{\mathcal{P}^5\sigma}^2 \\ 0 & -m_{\mathcal{P}^5\sigma}^2 & p^2 - m_\sigma^2 \end{pmatrix} , \tag{153}$$

$$iD_{\mathcal{S}^4\mathcal{S}^5\eta}^{-1}(p) = \begin{pmatrix} p^2 - m_{\mathcal{S}^4}^2 & 2i\mu_q p_0 & 0 \\ -2i\mu_q p_0 & p^2 - m_{\mathcal{S}^5}^2 & -m_{\mathcal{S}^5\eta}^2 \\ 0 & -m_{\mathcal{S}^5\eta}^2 & p^2 - m_\eta^2 \end{pmatrix} . \tag{154}$$

The former hadrons share $I = 0$ and 0^+, while the latter share $I = 0$ and 0^-.

Depicted in Figure 5 are the μ_q dependences of the mass of the 0^+ hadrons (left) and 0^- hadrons (right) with parameter set (150). Both figures indicate the stable μ_q dependences of the hadron masses in the hadronic phase, reflecting the so-called *Silver–Braze property*. In the baryon superfluid phase, meanwhile, notable behaviors are found. For instance, σ, B, and $\bar{B}$ mix, while η, B', and $\bar{B}'$ do not, due to the $U(1)_B$ violation. Among the σ-B-$\bar{B}$ mixed states, a massless mode is obtained, which corresponds to the NG boson accompanied by the $U(1)_B$ breaking. Additionally, the nonlinear mass suppression of the lightest mode of the η-B'-$\bar{B}'$ mixed state which was observed by the lattice simulation [41] is successfully reproduced, in contrast to the ChPT framework. From this reproduction, one can conclude that the present LSM is regarded as a plausible effective model which correctly describes the low-energy hadron spectrum in cold and dense QC$_2$D. For comparison, we exhibit the simulated mass spectra of iso-singlet $0^\pm$ hadrons at a finite μ_q in Figure 6, although some artifacts originating from a finite diquark source j contaminate the spectra. On the lattice, the mixings are indicated by the mass degeneracies. We note that the pion mass is analytically evaluated to be $m_\pi = 2\mu_q$, which is consistent with the lattice simulations [41].
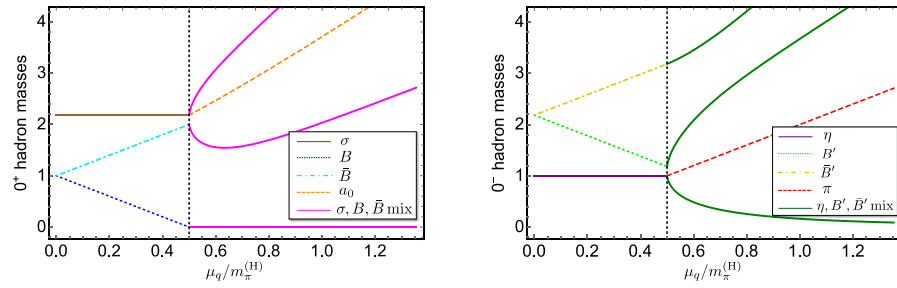
Figure 5. Mass spectra of 0^+ (**left**) and 0^- (**right**) hadrons evaluated within the present LSM. The masses are scaled by $m_\pi^{(H)}$. The figures are taken from Ref. [44] and legends are slightly modified.
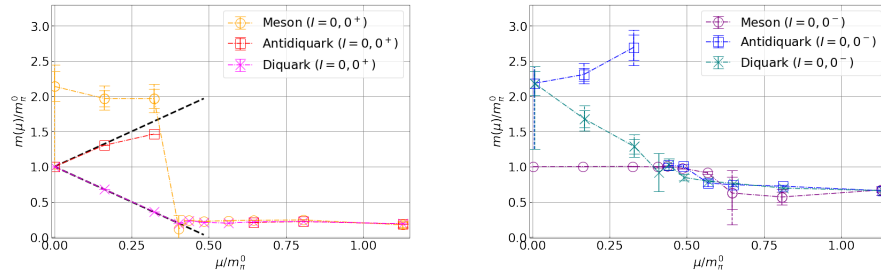
Figure 6. Mass spectra of 0^+ (**left**) and 0^- (**right**) iso-singlet hadrons measured on the lattice. The figures are taken from Ref. [41].

Quantitatively, the nonlinear suppression of the mass of the lightest η-B'-$\bar{B}'$ mixed state measured on the lattice is rather mild, while the present LSM result, in the absence of a $U(1)_A$ anomaly effect, exhibits a substantial mass reduction, as shown in Figures 5 and 6. In Ref. [44], it was demonstrated that as the $U(1)_A$ anomaly effects are enhanced within the LSM analysis, and the suppression is weakened so as to approach the correct behavior measured on the lattice. This observation suggests that the anomaly effects for hadrons are enhanced in the superfluid phase, while in the vacuum, the effects seem to be significantly suppressed. A similar anomaly enhancement at a finite density was also discussed with respect to three-color QCD by means of the functional renormalization group (FRG) method [81,82].

In Figure 7, we depict the mass spectrum of 0^+ and 0^- hadrons collectively for which mass degeneracies of the parity partners are clearly seen. At a sufficiently large μ_q, the mass degeneracies hold for the pairs (π, σ), (η, a_0), (B, B'), and $(\bar{B}, \bar{B}')$, where the mixings disappear.
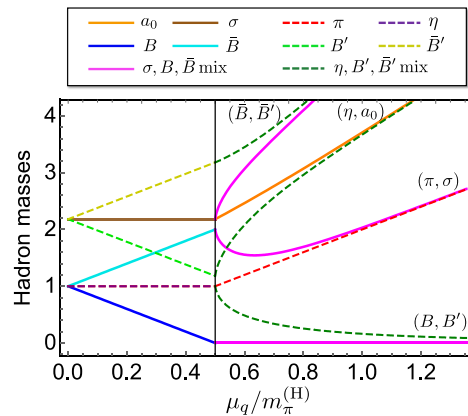
Figure 7. μ_q dependences of $0^\pm$ hadron masses. The figure is taken from Ref. [44], and legends are slightly modified.

4.4. LSM with a Diquark Source j

The inclusion of the diquark source *j* has no influence on the hadron mass formulas directly, but it modifies their effective potential, since *j* couples to Δ linearly, as in Equation (144). As a result, μ_q dependences of σ_0 and Δ are altered, as demonstrated in Figure 4, and accordingly, the hadron mass spectrum is changed.

Figure 8 exhibits the μ_q dependences of the hadron mass with $j = 0.2m_q$. For a finite *j*, Δ is always non-vanishing and σ-B-$\bar{B}$ mixing and η-B'-$\bar{B}'$ mixing occur at any μ_q. Additionally, the NG mode does not emerge since $U(1)_B$ symmetry is explicitly broken. The figure shows that the mass degeneracies between the chiral partners are clearly realized for a large μ_q.
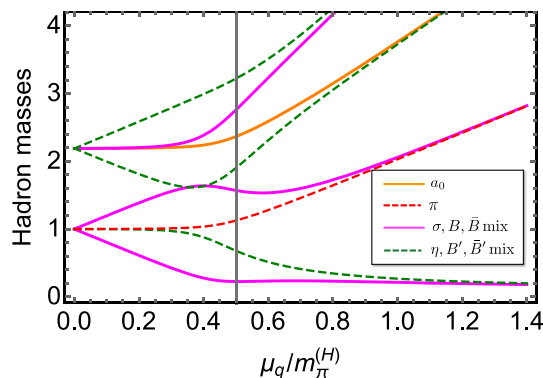

Figure 8. μ_q dependences of $0^{\pm}$ hadron masses with $j = 0.2m_q$.

In the following, we check the GOR relation analytically presented in Section 2.5 within the LSM. The broken current within the LSM is obtained by taking a derivative of $\mathcal{L}_{\mathrm{LSM}}^{\mathrm{eff}}$ with respect to $\zeta_{X\mu}^a \equiv -2\sqrt{2}V_\mu'^a$, as shown in Section 3.4, which yields

$$
\begin{aligned}
j_{X\mu}^a &= \frac{\sigma_0}{\sqrt{2}}\partial_\mu\pi^a + \cdots \quad (\text{for } a = 1-3)\,, \\
j_{X\mu}^4 &= \frac{\sigma_0}{\sqrt{2}}\partial_\mu\mathcal{P}^4 + \sqrt{2}\mu_q\sigma_0\delta_{\mu 0}\mathcal{P}^5 + \cdots \quad (\text{for } a = 4)\,, \\
j_{X\mu}^5 &= \frac{\sigma_0}{\sqrt{2}}\partial_\mu\mathcal{P}^5 - \frac{\Delta}{\sqrt{2}}\partial_\mu\sigma - \sqrt{2}\mu_q\sigma_0\delta_{\mu 0}\mathcal{P}^4 + \cdots \quad (\text{for } a = 5)\,.
\end{aligned}
\tag{155}
$$

Similarly, the $U(1)_B$ current is derived to be

$$
j_B^\mu = 2\Delta\partial_\mu\mathcal{P}^4 + 8\mu_q\Delta\delta_{\mu 0}\mathcal{P}^5 + \cdots\,,
\tag{156}
$$

by taking a derivative of the Lagrangian with respect to $\zeta_B^\mu \equiv V^{\mu,i=4}$. From the pion sector, immediately,

$$
f_\pi = \frac{\sigma_0}{\sqrt{2}}
\tag{157}
$$

is found by virtue of the definition of decay constant (52), regardless of its trivial sign. Thus, we can easily check the GOR relation for pions in Equation (66), from which the pion mass and chiral condensate are denoted by $m_\pi^2 = \sqrt{2}\bar{c}m_q/\sigma_0$ and Equation (143), respectively.

As for the baryonic sector, again, we take $\mu_q = 0$ to achieve concise relations. In the LSM framework, even in the vacuum, $\mathcal{P}^5$ and σ mix due to the baryon-number violation

that was absent in the ChPT analysis, as explicitly shown in Equation (153). The mixing is solved by introducing mass eigenstates $\tilde{\mathcal{P}}^5$ and $\tilde{\sigma}_0$ via

$$
\begin{pmatrix} \tilde{\mathcal{P}}^5 \\ \tilde{\sigma} \end{pmatrix} = \begin{pmatrix} \cos\vartheta & -\sin\vartheta \\ \sin\vartheta & \cos\vartheta \end{pmatrix} \begin{pmatrix} \mathcal{P}^5 \\ \sigma \end{pmatrix} , \tag{158}
$$

where the mixing angle ϑ is determined to satisfy $\tan\vartheta = \Delta/\sigma_0$ from Equation (153). The corresponding mass eigenvalues read

$$
m_{\tilde{\mathcal{P}}^5}^2 = m_\pi^2 \ , \quad m_{\tilde{\sigma}}^2 = m_\pi^2 + 2\tilde{\lambda}(\sigma_0^2 + \Delta^2) \ . \tag{159}
$$

Inverting mixing matrix (158), $\mathcal{P}^5$ and σ are expressed as a function of $\tilde{\mathcal{P}}^5$, and the current $j_{X\mu}^5$ in the vacuum in Equation (155) can be rewritten into

$$
j_{X\mu}^5 = \frac{\sigma_0\cos\theta + \Delta\sin\theta}{\sqrt{2}}\partial_\mu\tilde{\mathcal{P}}^5 + \cdots = \sqrt{\frac{\sigma_0^2 + \Delta^2}{2}}\partial_\mu\tilde{\mathcal{P}}^5 + \cdots , \tag{160}
$$

resulting in

$$
f_5 = \sqrt{\frac{\sigma_0^2 + \Delta^2}{2}} \ . \tag{161}
$$

Using $m_\pi^2 = \sqrt{2}\bar{c}m_q/\sigma_0 = \sqrt{2}\bar{c}j/\Delta$ at $\mu_q = 0$ and Equation (143), the GOR relation for the baryon in this limit, Equation (67), can be verified.

Finally, from Equation (156), the decay constant f_B is evaluated to be

$$
f_B = 2\Delta \tag{162}
$$

within the LSM. Meanwhile, $m_\pi^2 = \sqrt{2}j\bar{c}/\Delta$ at $\mu_q = 0$. Hence, using these equations together with Equation (143), one can confirm that the GOR relation associated with $U(1)_B$ symmetry (68) is certainly satisfied. (At a finite μ_q, $\left(\frac{f_B}{2\sqrt{2}}\right)^2 m_{B_4}^2 = -\frac{j\langle\psi\psi\rangle}{2}$ seems to hold, similarly to the ChPT framework).

4.5. Topological Susceptibility

The hadron mass spectrum from the LSM was presented in Section 4.3, indicating that the $U(1)_A$ anomaly effects in the superfluid phase are enhanced from the behavior of the lowest mode of the η-B'-$\bar{B}'$ mixed state. One of the useful quantities to explore within the $U(1)_A$ anomaly is the *topological susceptibility*, which is defined by

$$
\chi_{\text{top}} \equiv -i\int d^4x \frac{\delta^2\Gamma_{\text{QC}_2\text{D}}}{\delta\theta(x)\delta\theta(0)}\bigg|_{\theta=0} = -i\int d^4x \langle 0|\text{T}^*Q(x)Q(0)|0\rangle , \tag{163}
$$

since $Q = g_s^2/(64\pi^2)\epsilon^{\mu\nu\rho\sigma}G_{\mu\nu}^a G_{\rho\sigma}^a$ ($G_{\mu\nu}^a = \partial_\mu A_\nu^a - \partial_\nu A_\mu^a + g_s A_\mu^a A_\nu^b$ is the gluon field strength) is nothing but the topological charge responsible for the anomaly. Regarding the lattice, two groups, a Japanese group and a Russian group, have simulated the topological susceptibility at a finite μ_q [25,34,83]. However, those results seem to be inconsistent even on a qualitative level; the latter result indicates a suppression of χ_{top} at a large μ_q, while the former result exhibits a constant behavior. Thus, in this subsection, we investigate the topological susceptibility at a finite μ_q within the LSM to present useful information from a model study, and discuss the fate of the $U(1)_A$ anomaly effects in cold and dense QC$_2$D [70].

The QC$_2$D Lagrangian with the θ term is given by

$$\mathcal{L}_{\mathrm{QC_2D}} = \mathcal{L}^q_{\mathrm{QC_2D}} - \frac{1}{4}G^a_{\mu\nu}G^{\mu\nu a} + \theta\frac{g_s^2}{64\pi^2}\epsilon^{\mu\nu\rho\sigma}G^a_{\mu\nu}G^a_{\rho\sigma} \,, \tag{164}$$

where the quark part $\mathcal{L}^q_{\mathrm{QC_2D}}$ is defined by Equation (23). After a $U(1)_A$ transformation of $\psi \to \exp[(i\theta/4)\gamma_5]\psi$, Fujikawa's method [84] yields a modified Lagrangian as

$$\mathcal{L}^\theta_{\mathrm{QC_2D}} = \bar\psi i \slashed{D}\psi - m_q\bar\psi\exp[(i\theta/2)\gamma_5]\psi - \frac{1}{4}G^a_{\mu\nu}G^{\mu\nu a} \,, \tag{165}$$

whose θ dependence is now absorbed into the fermion mass term. Therefore, the topological susceptibility is evaluated to be

$$\chi_{\mathrm{top}} = -i\int d^4x \left.\frac{\delta^2\Gamma^\theta_{\mathrm{QC_2D}}}{\delta\theta(x)\delta\theta(0)}\right|_{\theta=0} = -\frac{1}{4}\left[m_q\langle\bar\psi\psi\rangle + im_q^2\chi_\eta\right]$$

$$= \frac{im_q^2}{4}(\chi_\pi - \chi_\eta)\,, \tag{166}$$

with $\Gamma^\theta_{\mathrm{QC_2D}} = -i\ln Z^\theta_{\mathrm{QC_2D}}$ being the effective action generated by the rotated QC$_2$D Lagrangian (165). In this equation, the meson susceptibilities are defined by

$$\chi_\eta = \int d^4x\langle 0|\mathrm{T}\mathcal{O}_\eta(x)\mathcal{O}_\eta(0)|0\rangle \,,$$

$$\chi_\pi\delta^{ab} = \int d^4x\langle 0|\mathrm{T}\mathcal{O}^a_\pi(x)\mathcal{O}^b_\pi(0)|0\rangle \,, \tag{167}$$

and the composite operators are defined in Equation (35). Additionally, in obtaining Equation (166), we have made use of

$$\langle\bar\psi\psi\rangle = -im_q\chi_\pi \,, \tag{168}$$

which is nothing but the first identity in Equation (56). Equation (166) indicates that the finite topological susceptibility is induced only when χ_η deviates from χ_π. These susceptibility functions are two-point functions of the corresponding composite operators with vanishing momentum. Thus, unless state mixings occur, they are essentially denoted by $\chi_\pi \propto -i/m_\pi^2$ and $\chi_\eta \propto -i/m_\eta^2$, where m_π and m_η are the pion and η meson masses. The difference between η mass and pion mass is generated by the $U(1)_A$ anomaly effect, so one can understand that the finite topological susceptibility is induced by the anomaly effect together with the current quark mass m_q [70].

The functions χ_π and χ_η are evaluated within the present LSM by virtue of matching condition (2). That is,

$$\chi_\eta = \frac{1}{i}\int d^4x\left.\frac{\delta^2\Gamma_{\mathrm{QC_2D}}}{\delta p^0(x)\delta p^0(0)}\right|_{\langle\zeta\rangle,\langle\zeta_\mu\rangle} = \frac{1}{i}\int d^4x\left.\frac{\delta^2\Gamma_{\mathrm{LSM}}}{\delta p^0(x)\delta p^0(0)}\right|_{\langle\zeta\rangle,\langle\zeta_\mu\rangle} = 2\bar c^2 D_\eta(0)\,, \tag{169}$$

and

$$\chi_\pi\delta^{ab} = \frac{1}{i}\int d^4x\left.\frac{\delta^2\Gamma_{\mathrm{QC_2D}}}{\delta p^a(x)\delta p^b(0)}\right|_{\langle\zeta\rangle,\langle\zeta_\mu\rangle} = \frac{1}{i}\int d^4x\left.\frac{\delta^2\Gamma_{\mathrm{LSM}}}{\delta p^a(x)\delta p^b(0)}\right|_{\langle\zeta\rangle,\langle\zeta_\mu\rangle} = 2\delta^{ab}\bar c^2 D_\pi(0)\tag{170}$$

$(a, b = 1 - 3)$, respectively, for which the spurious p^a were introduced in Section 2.3. In these equations, $D_\eta(p)$ and $D_\pi(p)$ are propagators of η and pion, respectively. Using these effective-model expressions, the topological susceptibility can be evaluated to be

$$\chi_{\text{top}} = \frac{i}{4} \left(m_\pi^{(\text{H})}\right)^2 \left(\sigma_0^{(\text{H})}\right)^2 \left(D_\pi(0) - D_\eta(0)\right) . \tag{171}$$

In the hadronic phase, these propagators are simply given by

$$D_\eta(p) = \frac{i}{p^2 - \left(m_\eta^{(\text{H})}\right)^2} \quad , \quad D_\pi(p) = \frac{i}{p^2 - \left(m_\pi^{(\text{H})}\right)^2} . \tag{172}$$

On the other hand, in the superfluid phase, $D_\eta(p)$ is contaminated by mixings among the η-B'-$\bar{B}$ (or η-$\mathcal{S}^4$-$\mathcal{S}^5$) modes due to the $U(1)$ baryon-number violation, but it is straightforwardly evaluated by picking up a D_η component by inverting the 3×3 matrix (154). The resultant μ_q dependences of the topological susceptibility with a vanishing diquark source j are depicted in the left panel of Figure 9. For this figure, we chose $m_\eta^{(\text{H})}/m_\pi^{(\text{H})} = 1.0, 1.05, 1.2, 1.5$ to take a closer look at the anomaly effect, where the anomaly effects are incorporated through the $\det\Sigma + \det\Sigma^\dagger$ term following Ref. [70]. The figure implies that the topological susceptibility is always vanishing when the anomaly effect is absent. When the anomaly effect is switched on, in the hadronic phase, a constant χ_{top} is induced, the magnitude of which is enhanced as we impose a stronger effect.
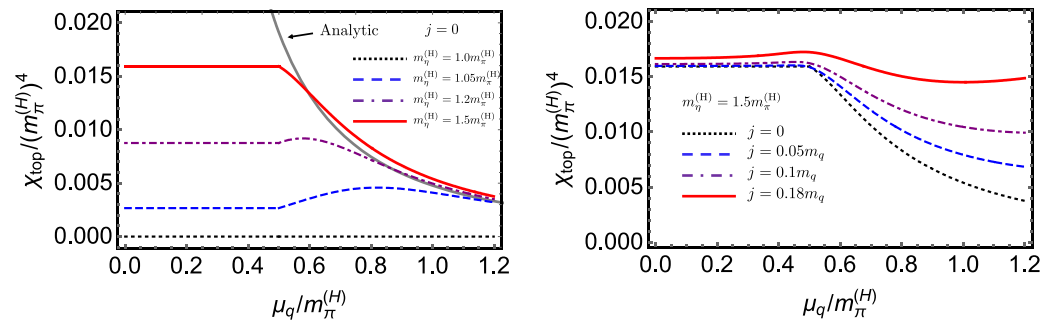
Figure 9. μ_q dependences of the topological susceptibility χ_{top} normalized by $\left(m_\pi^{(\text{H})}\right)^4$. The left and right panels show $m_\eta^{(\text{H})}/m_\pi^{(\text{H})}$ dependences with $j = 0$ and j dependences with $m_\eta^{(\text{H})}/m_\pi^{(\text{H})} = 1.5$, respectively.

The left panel of Figure 9 exhibits suppression of the topological susceptibility at a large μ_q, particularly for a larger $m_\eta^{(\text{H})}/m_\pi^{(\text{H})}$. To explore this behavior in detail, we rewrite Equation (166) in terms of the low-energy quantities. That is, with the help of GOR relationship (66), we can express the topological susceptibility (166) as

$$\chi_{\text{top}} = \frac{f_\pi^2 m_\pi^2}{2} \delta_m \quad \text{with} \quad \delta_m = 1 - \frac{\chi_\eta}{\chi_\pi} . \tag{173}$$

In this equation, f_π and m_π are the pion decay constant and pion mass in the superfluid phase, which read $f_\pi = \sigma_0/\sqrt{2}$ and $m_\pi = 2\mu_q$ within the present LSM, respectively. Using the asymptotic value of $\chi_\eta/\chi_\pi \sim 1/3$ [44] and an identity $f_\pi^2 m_\pi^4 = \left(f_\pi^{(\text{H})}\right)^2 \left(m_\pi^{(\text{H})}\right)^4$, one can approximate χ_{top} for a sufficiently large μ_q as

$$\chi_{\text{top}} \sim \frac{\left(f_\pi^{(\text{H})}\right)^2 \left(m_\pi^{(\text{H})}\right)^4}{3m_\pi^2} = \frac{\left(f_\pi^{(\text{H})}\right)^2 \left(m_\pi^{(\text{H})}\right)^4}{12} \mu_q^{-2} . \tag{174}$$

In the left panel of Figure 9, the black curve corresponds to this analytic solution, which is in good agreement with the numerical behaviors. Therefore, we conclude that the asymptotic suppression of the topological susceptibility is accompanied by an increment in pion mass, $m_\pi = 2\mu_q$ in the superfluid phase, i.e., chiral restoration.

In the actual lattice simulation, it is not so easy to take a zero limit of the diquark source, so it is worth studying the effects from the diquark source j within the LSM analysis. These effects are incorporated by $\langle p^0 \rangle = j$ for the spurion field, leading to

$$\chi_{\text{top}}^{\text{w}/j} = \chi_{\text{top}} + \delta\chi_{\text{top}} \,, \tag{175}$$

in which χ_{top} is defined in Equation (166) and the corrections driven by the diquark source read

$$\delta\chi_{\text{top}} = \frac{i}{2}m_q j \chi_{B_5'\eta} + \frac{i}{4}j^2(\chi_{B_4} - \chi_{B_5'}) \,. \tag{176}$$

The first contribution represents a mixed effect from the baryonic and mesonic sectors proportional to $m_q j$, while the second one shows a pure baryonic effect proportional to j^2, with the susceptibilities defined by

$$
\begin{aligned}
\chi_{B_5'\eta} &= \int d^4x \langle 0|T\mathcal{O}_\eta(x)\mathcal{O}_{B_5'}(0)|0\rangle \,, \\
\chi_{B_4} &= \int d^4x \langle 0|T\mathcal{O}_{B_4}(x)\mathcal{O}_{B_4}(0)|0\rangle \,, \\
\chi_{B_5'} &= \int d^4x \langle 0|T\mathcal{O}_{B_5'}(x)\mathcal{O}_{B_5'}(0)|0\rangle \,.
\end{aligned}
\tag{177}
$$

Here, we define the following composite operator of the negative-parity diquark:

$$\mathcal{O}_{B_5'} = -\frac{1}{2}\psi^T C \tau_c^2 \tau_f^2 \psi + \text{H.c.} \,. \tag{178}$$

Susceptibility functions (177) can be evaluated within the LSM framework similarly to Equations (169) and (170).

The resultant topological susceptibilities with $j/m_q = 0, 0.05, 0.1, 0.18$ and $m_\eta^{(H)}/m_\pi^{(H)} = 1.5$ are exhibited in the right panel of Figure 9. As j increases, the suppression of χ_{top} diminishes. In particular, when $j/m_q = 0.18$, the topological susceptibility is approximately constant in a range of $0 < \mu_q \lesssim 1.2m_\pi^{(H)}$.
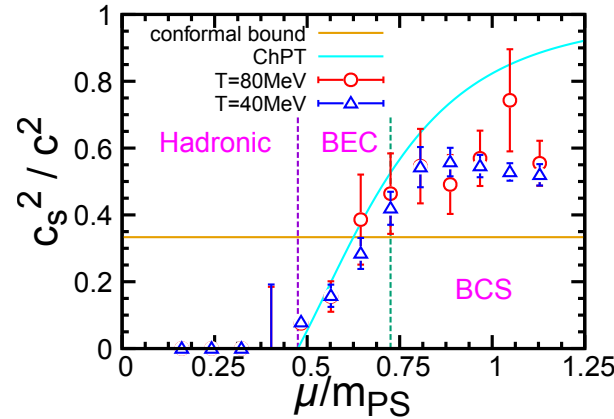
4.6. Sound Velocity

Recently, the sound velocity at a low temperature was simulated on the lattice [30,34], as exhibited in Figure 10, indicating that the sound velocity exceeds the conformal limit $\bar{c}_s^2 = 1/3$ for $\mu_q \gtrsim 0.7m_\pi^{(H)}$. Meanwhile, we know that, finally, it must converge on the limiting value $\bar{c}_s^2$ from the following simple dimensional analysis. When the chemical potential is sufficiently large, $\mu_q \gg \Lambda_{\text{QC}_2\text{D}}$, the pressure p takes the form of (α is some constant)

$$p \sim \alpha\mu_q^4 \,, \tag{179}$$

since the system is dominated by only μ_q. Hence, the number density and its susceptibility are derived to be $n = 4\alpha\mu_q^3$ and $\chi = 12\alpha\mu_q^2$, resulting in

$$c_s^2 \sim \frac{4\alpha\mu_q^3}{\mu_q \times 12\alpha\mu_q^2} = \frac{1}{3} \,, \tag{180}$$

with the help of formula (121). Therefore, the lattice result implies the existence of peak structures of c_s^2 at some μ_q.

Figure 10. The lattice result on the sound velocity at a finite chemical potential. This figure is taken from Ref. [34].

As investigated in Section 3.5, the sound velocity evaluated within the ChPT exceeds the conformal value $\bar{c}_s^2 = 1/3$ but monotonically approaches $c_s^2 \sim 1$ at a large μ_q without exhibiting any peaks [10,77]. This behavior contradicts the above simple dimensional analysis. This contradiction emerges because the ChPT framework is constructed upon the manifold of G/H, which requires a definite energy scale to break certain symmetries. In fact, pressure (118) is always proportional to the decay constant f_0. On the other hand, the LSM is based on a linear representation of the Pauli–Gürsey $SU(4)$ symmetry which naturally allows us to enter the symmetry restored phase. Thus, there is no intrinsic energy scale to characterize the symmetry breaking, and the correct asymptotic behavior of the sound velocity is expected to be reproduced. Keeping this expectation in mind, here, we examine the sound velocity within the LSM, particularly focusing on the influence from the chiral partner structure, as an extended model of the ChPT.

From the effective potential (144), the appropriately subtracted pressure derived within the LSM is evaluated to be [72]

$$p_{\text{LSM}}^{\text{sub}} = p_{\text{ChPT}}^{\text{sub}} + \delta p \,, \tag{181}$$

where $p_{\text{ChPT}}^{\text{sub}}$ is the subtracted pressure from the ChPT (118). The additional contribution δp is ($\bar{\mu} = \mu_q/\mu_{\text{cr}} = 2\mu_q/m_\pi^{(\text{H})}$)

$$\delta p = \left(f_\pi^{(\text{H})}\right)^2 \left(m_\pi^{(\text{H})}\right)^2 \left[\frac{4}{\delta \bar{m}_{\sigma-\pi}^2}(\bar{\mu}^2 - 1)^2\right] \,, \tag{182}$$

with

$$\delta \bar{m}_{\sigma-\pi}^2 = \frac{\left(m_\sigma^{(\text{H})}\right)^2 - \left(m_\pi^{(\text{H})}\right)^2}{\mu_{\text{cr}}^2} \,, \tag{183}$$

and $f_\pi^{(\text{H})} = \sigma_0^{(\text{H})}/\sqrt{2}$. In this equation,

$$\begin{aligned}
\left(m_\pi^{(\text{H})}\right)^2 &= m_0^2 + \tilde{\lambda}\left(\sigma_0^{(\text{H})}\right)^2 \,, \\
\left(m_\sigma^{(\text{H})}\right)^2 &= m_0^2 + 3\tilde{\lambda}\left(\sigma_0^{(\text{H})}\right)^2 \,,
\end{aligned} \tag{184}$$

are the masses of the pion and sigma meson in the hadronic phase, so that

$$\delta \bar{m}^2_{\sigma - \pi} = \frac{2\tilde{\lambda}\left(\sigma_0^{(\mathrm{H})}\right)^2}{\mu_{\mathrm{cr}}^2} \ . \tag{185}$$

Thus, in a limit of $\mu_q \to \infty$, we can see $\delta p \to \mu_q^4/\tilde{\lambda}$, which dominates over the ChPT result $p_{\mathrm{ChPT}}^{\mathrm{sub}}$, and

$$p_{\mathrm{LSM}}^{\mathrm{sub}} \to \frac{1}{\tilde{\lambda}}\mu_q^4 \ . \tag{186}$$

This scaling is indeed consistent with the simple dimensional analysis (179). Notably, the correction (182) is proportional to the inverse of the chiral partner mass difference $\delta \bar{m}^2_{\sigma - \pi}$. In a limit of $m_\sigma^{(\mathrm{H})} \to \infty$, δp vanishes and the pressure is reduced to $p_{\mathrm{ChPT}}^{\mathrm{sub}}$, which is consistent with a fact that integrating out the σ meson from the LSM derives the ChPT.

From the pressure (181) and the energy density, the number density and its susceptibility are readily obtained in the following forms,

$$\begin{aligned}
\epsilon_{\mathrm{LSM}}^{\mathrm{sub}} &= \epsilon_{\mathrm{ChPT}}^{\mathrm{sub}} + \delta\epsilon \ , \\
n_{\mathrm{LSM}}^{\mathrm{sub}} &= n_{\mathrm{ChPT}}^{\mathrm{sub}} + \delta n \ , \\
\chi_{\mathrm{LSM}}^{\mathrm{sub}} &= \chi_{\mathrm{ChPT}}^{\mathrm{sub}} + \delta\chi \ ,
\end{aligned} \tag{187}$$

with the corrections evaluated as

$$\begin{aligned}
\delta\epsilon &= \left(f_\pi^{(\mathrm{H})}\right)^2 \left(m_\pi^{(\mathrm{H})}\right)^2 \left[\frac{4}{\delta\bar{m}^2_{\sigma-\pi}}(3\bar{\mu}^2+1)(\bar{\mu}^2-1)\right] \ , \\
\delta n &= \frac{2\left(f_\pi^{(\mathrm{H})}\right)^2 \left(m_\pi^{(\mathrm{H})}\right)^2}{\mu_q}\left[\frac{8}{\delta\bar{m}^2_{\sigma-\pi}}(\bar{\mu}^4-\bar{\mu}^2)\right] \ , \\
\delta\chi &= 8\left(f_\pi^{(\mathrm{H})}\right)^2 \left[\frac{8}{\delta\bar{m}^2_{\sigma-\pi}}(3\bar{\mu}^2-1)\right] \ .
\end{aligned} \tag{188}$$

All these corrections vanish when taking $m_\sigma \to \infty$ to reproduce the corresponding ChPT results. The resultant sound velocity is given by

$$\left(c_s^{\mathrm{LSM}}\right)^2 = \frac{n_{\mathrm{ChPT}} + \delta n}{\mu_q(\chi_{\mathrm{ChPT}} + \delta\chi)} = \frac{(1-1/\bar{\mu}^4) + 8(\bar{\mu}^2-1)/\delta\bar{m}^2_{\sigma-\pi}}{(1+3/\bar{\mu}^4) + 8(3\bar{\mu}^2-1)/\delta\bar{m}^2_{\sigma-\pi}} \ . \tag{189}$$

Depicted in Figure 11 is the μ_q dependence of the sound velocity (189), with $m_\sigma^{(\mathrm{H})}/m_\pi^{(\mathrm{H})} = 2, 5, 20$ and ∞. The gray dashed line is an analytic solution expanded in the vicinity of $\mu_q \approx \mu_{\mathrm{cr}}$ in Equation (189), $c_s^2 \approx \bar{\mu} - 1$, which is independent of $m_\sigma^{(\mathrm{H})}$. This figure shows that the sound velocity peak is successfully reproduced within the present LSM, where the chiral partner contribution proportional to $1/\delta\bar{m}^2_{\sigma-\pi}$ is incorporated [72]. Thus, from this reproduction, one can conclude that the LSM is capable of accessing a more dense region of QC$_2$D, where the ChPT cannot be applied. For quantitative comparisons, it is inevitable to include fluctuations and spin-1-hadron contributions.
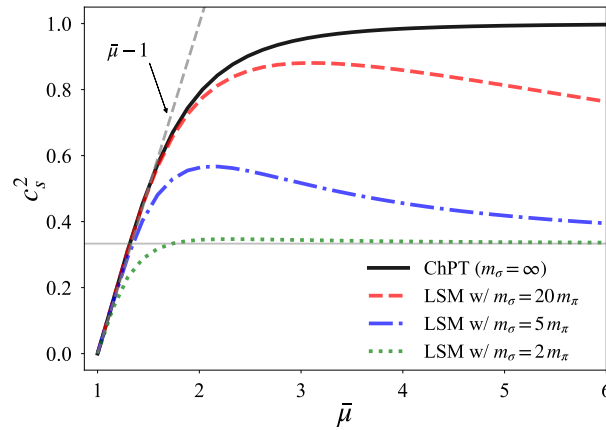
Figure 11. $\bar{\mu}$ $(=$ $\mu_q/\mu_{\rm cr}$ $=$ $2\mu_q/m_\pi^{(\rm H)})$ dependences of the sound velocity c_s^2 with $m_\sigma^{(\rm H)}/m_\pi^{(\rm H)} = 2, 5, 20, \infty$. The dashed gray line denotes $c_s^2 = \bar{\mu} - 1$, evaluated analytically. This figure is taken from Ref. [72].

5. Extended Linear Sigma Model (eLSM)

5.1. Model Construction

In Section 4.3, the mass spectra of negative-parity and positive-parity spin-0 hadrons in cold and dense QC_2D were explored within the LSM framework, and μ_q dependences of the hadron masses were elucidated from a symmetry viewpoint. Meanwhile, the lattice simulation indicates the flipping of the mass ordering, where the pion becomes heavier than the ρ meson in the superfluid phase [11,41]. This behavior implies that a model analysis including spin-1 hadrons is inevitable to further correctly explore the low-energy physics of dense QC_2D. Thus, here, we invent the eLSM, describing spin-0 and spin-1 hadrons in a unified way based on the linear representation of the Pauli–Gürsey $SU(4)$ symmetry [71]. (The eLSM in three-color QCD was invented by the Frankfurt group [85,86]).

Employing the linear representation, the interpolating fields of the low-lying spin-1 mesons and baryons are given by

$$\omega^\mu \sim \bar\psi \gamma^\mu \psi \,, \quad f_1^\mu \sim \bar\psi \gamma_5 \gamma^\mu \psi \,, \quad \rho^{0,\mu} \sim \bar\psi \tau_f^3 \gamma^\mu \psi \,,$$

$$\rho^{\pm,\mu} \sim \frac{1}{\sqrt{2}} \bar\psi \tau_f^\mp \gamma^\mu \psi \,, \quad a_1^{0,\mu} \sim \bar\psi \tau_f^3 \gamma_5 \gamma^\mu \psi \,, \quad a_1^{\pm,\mu} \sim \frac{1}{\sqrt{2}} \bar\psi \tau_f^\mp \gamma_5 \gamma^\mu \psi \,, \tag{190}$$

and

$$B_S^{I_z=0,\mu} \sim -\frac{i}{\sqrt{2}} \psi^T \mathcal{C} \gamma^\mu \tau_c^2 \tau_f^1 \psi \,, \quad B_S^{I_z=\pm1,\mu} \sim -\frac{i}{2} \psi^T \mathcal{C} \gamma^\mu \tau_c^2 (\mathbf{1}_f \pm \tau_f^3) \psi \,,$$

$$B_{AS}^\mu \sim -\frac{1}{\sqrt{2}} \psi^T \mathcal{C} \gamma_5 \gamma^\mu \tau_c^2 \tau_f^2 \psi \,, \quad \bar{B}_S^{I_z=0,\pm1,\mu} = (B_S^{I_z=0,\pm1,\mu})^\dagger \,, \quad \bar{B}_{AS}^\mu = (B_{AS}^\mu)^\dagger \,, \tag{191}$$

respectively, the quantum numbers of which are summarized in Table 2. Thus, a useful 4×4 matrix describing the quark bilinear fields of the spin-1 hadrons is introduced as

$$\Phi_{ij}^\mu \sim \Psi_j^\dagger \sigma^\mu \Psi_i \,, \tag{192}$$

as a sibling of Σ in Equation (133), for which the hadron fields can be embedded in the following manner,

$$
\Phi^\mu = \frac{1}{2}\begin{pmatrix} \frac{\omega+\rho^0-(f_1+a_1^0)}{\sqrt{2}} & \rho^+ - a_1^+ & \sqrt{2}B_S^{I_z=+1} & B_S^{I_z=0} - B_{AS} \\ \rho^- - a_1^- & \frac{\omega-\rho^0-(f_1-a_1^0)}{\sqrt{2}} & B_S^{I_z=0} + B_{AS} & \sqrt{2}B_S^{I_z=-1} \\ \sqrt{2}\bar{B}_S^{I_z=-1} & \bar{B}_S^{I_z=0} + \bar{B}_{AS} & -\frac{\omega+\rho^0+f_1+a_1^0}{\sqrt{2}} & -(\rho^- + a_1^-) \\ \bar{B}_S^{I_z=0} - \bar{B}_{AS} & \sqrt{2}\bar{B}_S^{I_z=+1} & -(\rho^+ + a_1^+) & -\frac{\omega-\rho^0+f_1-a_1^0}{\sqrt{2}} \end{pmatrix}^\mu , \tag{193}
$$

from Equations (190) and (191). This matrix is reduced to

$$
\Phi^\mu = \left(\sum_{i=1}^{10} V^i S^i - \sum_{a=0}^{5} V'^a X^a\right)^\mu \tag{194}
$$

such that symmetry properties of the spin-1 hadrons become clear when assigning the hadron fields as

$$
\omega = V^0 , \quad \rho^\pm = \frac{V^1 \mp iV^2}{\sqrt{2}} , \quad \rho^0 = V^3 , \quad f_1 = V'^0 , \quad a_1^\pm = \frac{V'^1 \mp iV'^2}{\sqrt{2}} , \quad a_1^0 = V'^3 ,
$$

$$
B_S^{I_z=0} = \frac{V^9 + iV^{10}}{\sqrt{2}} , \quad \bar{B}_S^{I_z=0} = \frac{V^9 - iV^{10}}{\sqrt{2}} , \quad B_S^{I_z=\pm1} = \frac{(V^5 + iV^6) \pm (V^7 + iV^8)}{2} ,
$$

$$
\bar{B}_S^{I_z=\pm1} = \frac{(V^5 - iV^6) \mp (V^7 - iV^8)}{2} , \quad B_{AS} = \frac{V'^5 - iV'^4}{\sqrt{2}} , \quad \bar{B}_{AS} = \frac{V'^5 + iV'^4}{\sqrt{2}} . \tag{195}
$$

The Pauli–Gürsey $SU(4)$ transformation law of Φ^μ is

$$
\Phi^\mu \to g\Phi^\mu g^\dagger \quad \text{with} \quad g \in SU(4) , \tag{196}
$$

from Equation (192).

Table 2. Quantum numbers of the spin-1 hadrons.

Hadron	Spin and Parity (J^P)	Quark Number	Isospin
ω	1^-	0	0
ρ	1^-	0	1
f_1	1^+	0	0
a_1	1^+	0	1
B_S ($\bar{B}_S$)	1^+	$+2(-2)$	1
B_{AS} ($\bar{B}_{AS}$)	1^-	$+2(-2)$	0

From transformation laws (136) and (196), an effective Lagrangian describing the low-lying spin-0 and spin-1 hadrons of QC$_2$D comprehensively, i.e., the eLSM Lagrangian, is readily obtained as [71]

$$
\begin{aligned}
\mathcal{L}_{\text{eLSM}} = & \ \text{tr}[D_\mu\Sigma^\dagger D^\mu\Sigma] - m_0^2\text{tr}[\Sigma^\dagger\Sigma] - \lambda_1\big(\text{tr}[\Sigma^\dagger\Sigma]\big)^2 - \lambda_2\text{tr}[(\Sigma^\dagger\Sigma)^2] \\
& + \bar{c}\,\text{tr}[\zeta^\dagger\Sigma + \Sigma^\dagger\zeta] + \mathcal{L}_{\text{anom.}} - \frac{1}{2}\text{tr}[\Phi_{\mu\nu}\Phi^{\mu\nu}] + m_1^2\text{tr}[\Phi_\mu\Phi^\mu] \\
& + ig_3\text{tr}\big[\Phi_{\mu\nu}[\Phi^\mu,\Phi^\nu]\big] + h_1\text{tr}[\Sigma^\dagger\Sigma]\text{tr}[\Phi_\mu\Phi^\mu] + h_2\text{tr}[\Sigma\Sigma^\dagger\Phi_\mu\Phi^\mu] \\
& + h_3\text{tr}[\Phi_\mu^T\Sigma^\dagger\Phi^\mu\Sigma] + g_4\text{tr}[\Phi_\mu\Phi_\nu\Phi^\mu\Phi^\nu] + g_5\text{tr}[\Phi_\mu\Phi^\mu\Phi_\nu\Phi^\nu] \\
& + g_6\text{tr}[\Phi_\mu\Phi^\mu]\text{tr}[\Phi_\nu\Phi^\nu] + g_7\text{tr}[\Phi_\mu\Phi_\nu]\text{tr}[\Phi^\mu\Phi^\nu] .
\end{aligned} \tag{197}
$$

In this Lagrangian,

$$\Phi_{\mu\nu} \equiv D_\mu \Phi_\nu - D_\nu \Phi_\mu \tag{198}$$

is a field strength for the spin-1 hadrons, and the covariant derivatives for Σ and Φ take the forms of

$$
\begin{aligned}
D_\mu \Sigma &\equiv \partial_\mu \Sigma - i\zeta_\mu \Sigma - i\Sigma\zeta_\mu^T - ig_1\Phi_\mu\Sigma - ig_2\Sigma\Phi_\mu^T \, , \\
D_\mu \Phi_\nu &\equiv \partial_\mu \Phi_\nu - i[\zeta_\mu, \Phi_\nu] \, ,
\end{aligned}
\tag{199}
$$

respectively, with the spurion field ζ^μ. It should be noted that

$$
\begin{aligned}
&\mathrm{tr}[D_\mu \Sigma^\dagger D^\mu \Sigma] + h_2 \mathrm{tr}[\Sigma\Sigma^\dagger \Phi_\mu \Phi^\mu] + h_3 \mathrm{tr}[\Phi_\mu^T \Sigma^\dagger \Phi^\mu \Sigma] \\
=\ &\mathrm{tr}[\partial_\mu \Sigma^\dagger \partial^\mu \Sigma] + (g_1 + g_2)\mathrm{tr}[\Sigma\Sigma^\dagger\{\Phi_\mu, \zeta^\mu\}] + 2(g_1 + g_2)\mathrm{tr}[\Phi_\mu^T \Sigma^\dagger \zeta^\mu \Sigma] \\
+\ &i(g_1 + g_2)\mathrm{tr}[\Phi_\mu(\partial^\mu \Sigma\Sigma^\dagger - \Sigma\partial^\mu\Sigma^\dagger)] + (g_1^2 + g_2^2 + h_2)\mathrm{tr}[\Sigma\Sigma^\dagger\Phi_\mu\Phi^\mu] \\
+\ &(2g_1 g_2 + h_3)\mathrm{tr}[\Phi_\mu^T \Sigma^\dagger \Phi^\mu \Sigma]
\end{aligned}
\tag{200}
$$

holds, from which $\Sigma^T = -\Sigma$, implying that the four parameters g_1, g_2, h_2, and h_3 can be rearranged into the following three:

$$
\begin{aligned}
C_1 &\equiv g_1 + g_2 \, , \\
C_2 &\equiv g_1^2 + g_2^2 + h_2 \, , \\
C_3 &\equiv 2g_1 g_2 + h_3 \, .
\end{aligned}
\tag{201}
$$

The eLSM Lagrangian (197) effectively contains 14 parameters, regardless of the anomalous contributions, which are hard to be completely fixed due to the current limited lattice results. Here, to pick up only the leading contributions, first, we assume the large N_c limit that would be also supported by the so-called Zweig rule for spin-1 sectors. Thus, $\lambda_1 = h_1 = g_6 = g_7 = 0$. Also, we again ignore the anomaly effects. Next, we assume $C \equiv C_1 = C_2$ since those parameters essentially play the same role, controlling the mixings between the spin-0 and spin-1 hadrons. Then, as for the couplings among spin-1 hadrons, we employ the following relations,

$$g_3 = g_\Phi \, , \quad g_4 = -g_5 = g_\Phi^2 \, , \tag{202}$$

which can be inferred by the $\mathcal{O}(p^2)$ contributions of the HLS formalism [52]. After those reductions, seven free parameters are left.

5.2. Hadron Mass Spectrum

In this subsection, we investigate the μ_q dependences of the spin-1 hadron masses predicted by our eLSM.

To delineate the hadron mass spectrum, we need to take into account the mean field contributions appropriately. In the present analysis, we assume the following four mean fields:

$$\sigma_0 = \langle \sigma \rangle \, , \quad \Delta = \langle B^5 \rangle \, , \quad \bar{\omega} = \langle \omega_{\mu=0} \rangle \, , \quad \bar{V} = \langle V'^4_{\mu=0} \rangle \, . \tag{203}$$

The spin-0 mean fields σ_0 and Δ correspond to the chiral and diquark condensates, respectively, similarly to the analysis in Section 4.3. The third one, $\bar{\omega}$, is a mean field of the ω meson modifying the chemical potential effects. The last one, $\bar{V}$, is responsible for a mean field of the iso-singlet and vector diquark, which is allowed due to the $U(1)_B$ violation

in the baryon superfund phase. The configuration of those mean fields is determined by solving each the stationary condition. The resultant gap equations are rather complicated, so we leave their concrete forms to Ref. [71].

In the following numerical analysis, we adopt

$$m_\rho^{(\mathrm{H})} = 908\,\mathrm{MeV}\,,\quad m_{a_1}^{(\mathrm{H})} = 1614\,\mathrm{MeV}\,, \tag{204}$$

as inputs associated with the spin-1 hadron masses simulated on the lattice [41,79], in addition to inputs (148) and (149). Hence, there remain only two free parameters, C and g_Φ. When choosing $C = 12$, the μ_q dependences of the mean fields (203) can be determined as exhibited in Figure 12, regardless of the value of g_Φ.
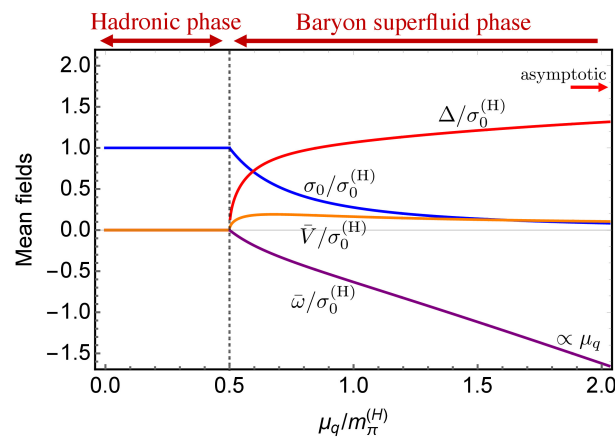

Figure 12. μ_q dependences of the four mean fields: σ_0, Δ, $\bar{\omega}$, and $\bar{V}$. The figure is taken from Ref. [71].

Figure 12 indicates that only σ_0 is finite in the hadronic phase, whereas the remaining mean fields are always vanishing there. In the superfluid phase induced by a nonzero Δ, the spin-1 mean fields $\bar{\omega}$ and $\bar{V}$ also acquire non-vanishing values. In particular, $\bar{\omega}$ grows linearly with respect to μ_q. Meanwhile, the gap Δ converges on a certain value at a sufficiently large μ_q, which is indicated by the arrow in this figure. The remaining mean fields σ_0 and $\bar{V}$ asymptotically vanish for $\mu_q \to \infty$. It should be noted that the critical chemical potential to enter the baryon superfluid phase is again given by $\mu_{\mathrm{cr}} = m_\pi^{(\mathrm{H})}/2$, as the other chiral effective models predict, as long as we take into account the additional two spin-1 meson fields correctly.

We are now ready to examine the hadron mass spectra of the spin-1 hadrons at a finite μ_q, since their mass formulas are straightforwardly obtained by reading off the quadratic terms from the reduced eLSM Lagrangian. The resulting formulas are complicated due to considerable mixings, so we do not present those here. (For details, please see the Appendices of Ref. [71]).

Depicted in Figures 13 and 14 are the spin-1 hadron mass spectra with $(g_\Phi, C) = (10, 12)$ and $(g_\Phi, C) = (10, 8)$, respectively, where the parameters are tuned to reproduce the mass reduction of the ρ meson in the superfluid phase measured on the lattice. The figures indicate that all the spin-1 hadron masses are constant or just linearly corrected with μ_q in the hadronic phase, similarly to the spin-0 meson masses. In the superfluid phase, meanwhile, several nonlinear behaviors are obtained due to state mixings from the $U(1)_B$ violation; the three pink curves in the left panels denote the ω-B_{AS}-$\bar{B}_{\mathrm{AS}}$ mixed stats, while the green ones in the right panels denote the a_1-B_{S}-$\bar{B}_{\mathrm{S}}$ mixed stats. In Figure 14, the colored area represents the axialvector condensed phase triggered by the mass of the lowest state of the a_1-B_{S}-$\bar{B}_{\mathrm{S}}$ mixed mode, which converges on zero. The possibility of the (axial)vector condensations was also predicted in Ref. [45], although the gap equation to determine the

ground-state configuration was not solved consistently. Thus, it would be challenging to seek for such $SO(3)$-violating phases in future lattice simulations.
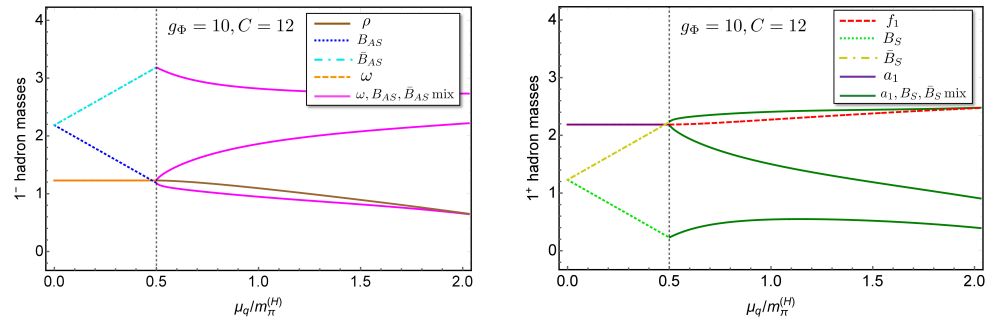

Figure 13. μ_q dependences of the 1^- (**left**) and 1^+ (**right**) hadron masses with $g_\Phi = 10$ and $C = 12$. The figures are taken from Ref. [71].
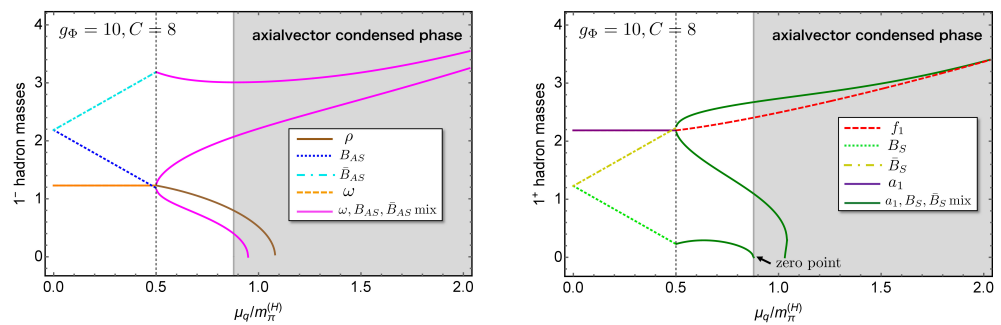
Figure 14. μ_q dependences of the 1^- (**left**) and 1^+ (**right**) hadron masses with $g_\Phi = 10$ and $C = 8$. The figures are taken from Ref. [71].

The mass degeneracies between the parity partners, i.e., chiral partners, are realized among the spin-1 hadrons, similarly to the spin-0 hadrons. To see this behavior, we show the μ_q dependences of the masses of all $1^\pm$ hadrons in Figure 15. For this figure, we adopted $(g_\Phi, C) = (10, 16)$ to clearly confirm the mass degeneracies and plotted them up to $\mu_q = 2.5$. This figure indicates that the degeneracies hold for (B_S, B_{AS}), (ρ, a_1), (ω, f_1), and $(\bar{B}_S, \bar{B}_{AS})$.
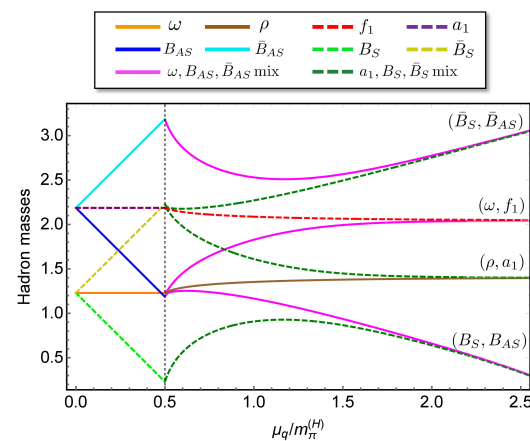
Figure 15. μ_q dependences of all the spin-1 hadron masses. We employed $(g_\Phi, C) = (10, 16)$ to see the mass degeneracies of the chiral partners clearly. This figure is taken from Ref. [71].

6. Conclusions

In this review, I summarized the main points of recent works on cold and dense QC$_2$D by means of the LSM, which is capable of describing the low-energy hadron spectrum in the baryon superfluid phase correctly [44,70–72], as an extension of the ChPT.

As for the spin-0 hadron mass spectrum, in the baryon superfluid phase, the LSM yielded a massless (the lowest) mode in the iso-singlet 0^+ system, which can be regarded as the NG boson of $U(1)_B$ symmetry breaking. Additionally, a nonlinearly suppressed second-lowest mode was found in the iso-singlet 0^- system. Those lowest-lying behaviors are qualitatively consistent with the lattice results. From a quantitative comparison of the latter nonlinear mass suppression, an enhancement of the $U(1)_A$ anomaly effects on the hadrons was predicted. The mass spectrum of $0^\pm$ hadrons and some GOR relationships in the presence of the diquark source were also newly evaluated.

As for the spin-1 hadron mass spectrum, we found several parameter sets for which the ρ meson mass reduction in the superfluid phase observed by the lattice simulation is reproduced. Then, a possibility of the (axial)vector condensations violating the $SO(3)$ rotational symmetry was discussed. For both the spin-0 and spin-1 hadrons, mass degeneracies between the parity partners, i.e., the chiral partner structure, at higher densities were predicted.

Our WTI-based LSM analysis implies that topological susceptibility in cold and dense QC$_2$D is suppressed, followed by chiral symmetry restoration. If the $U(1)_A$ anomaly effect is assumed to be enhanced in such dense system, however, the suppression is weakened. Thus, the fate of the topological susceptibility largely depends on the behavior of the $U(1)_A$ anomaly on a hadronic level.

We also observed that the peak structure of a (squared) sound velocity in the superfluid phase can be successfully reproduced within our LSM framework, whereas the ChPT analysis cannot. This fact, in addition to the reproduction of the low-energy hadron spectrum in the superfluid phase, implies that the LSM constructed upon the linear representation of quark fields is applicable in the deeper region of the crossover from hadronic to quark matter.

In the following, I will present some topics related to the QC$_2$D study. Similarly to QC$_2$D, the isospin QCD (QCD$_I$) where the isospin chemical potential is included, can also be regarded as a useful testing ground aiming toward the elucidation of cold and dense QCD, thanks to disappearance of the sign problem in lattice simulations [77,87–93]. The present LSM is easily translated into the QCD$_I$ language; hence, dense QCD$_I$ is another field helpful in checking the results harvested from the LSM analysis in QC$_2$D. Examinations in these systems are expected to provide useful information on the equations of the state of dense matter, which are crucial to explain the observation data of neutron stars [94,95].

QC$_2$D is not only useful for delineating cold and dense QCD but also related to dark matter candidates, such as strongly interacting massive particles [96–102]. In this regard, it would be intriguing whether the present LSM is capable of contributing to those beyond standard analyses.

QC$_2$D has the advantage that (anti)diquarks are counted as color-singlet hadrons, while in three-color QCD, they cannot be directly observed. In the latter real-life application, diquark properties play an important role in determining the chiral dynamics of singly heavy baryons (SHBs) made of a heavy quark and a diquark, by virtue of the heavy quark effective theory [103]. Thus, the examination of diquarks in QC$_2$D through both theoretical and lattice studies is expected to provide useful information on SHB spectroscopy, e.g., the so-called "inverse mass hierarchy" induced by the $U(1)_A$ anomaly for the unobserved chiral partner SHBs [104–106]. As long as we stick to zero chemical potential, lattice simulations with $2 + 1$ flavors are straightforward for any number of color. (In three-color QCD, lattice studies on diquarks by means of, e.g., gauge-fixing treatment, potential problems, and static color-source methods, are being conducted [107–112].) In this regard, lattice simulations focusing on diquarks in QC$_2$D with $N_f = 2 + 1$ are a challenging issue

toward the elucidation of SHB properties in our world, considering chiral symmetry and the $U(1)_A$ anomaly.

Those applications imply that, although QC$_2$D is a "virtual" theory affected by QCD-like quarks and gluons, plenty of benefits are expected broadly, not to mention the numerical experiments in cold and dense media.

Data Availability Statement: Not applicable.

Conflicts of Interest: The author declares no conflicts of interest.

Abbreviations

The following abbreviations are used in this manuscript:

BCS	Bardeen–Cooper–Schrieffer
BEC	Bose–Einstein condensation
ChPT	Chiral perturbation theory
ELSM	Extended linear sigma model
GOR	Gell–Mann–Oakes–Renner
LHS	Left-hand side
LSM	Linear sigma model
NG	Nambu–Goldstone
QCD	Quantum chromodynamics
QC$_2$D	Two-color QCD
QCD$_I$	Isospin QCD
RHS	Right-hand side
SHB	Singly heavy baryon
VEV	Vacuum expectation value
WTI	Ward–Takahashi identity

References

1. Baym, G.; Hatsuda, T.; Kojo, T.; Powell, P.D.; Song, Y.; Takatsuka, T. From hadrons to quarks in neutron stars: A review. *Rept. Prog. Phys.* **2018**, *81*, 056902. [CrossRef] [PubMed]
2. Aarts, G. Introductory lectures on lattice QCD at nonzero baryon number. *J. Phys. Conf. Ser.* **2016**, *706*, 022004. [CrossRef]
3. Nagata, K. Finite-density lattice QCD and sign problem: Current status and open problems. *Prog. Part. Nucl. Phys.* **2022**, *127*, 103991. [CrossRef]
4. Hands, S.; Kogut, J.B.; Lombardo, M.P.; Morrison, S.E. Symmetries and spectrum of SU(2) lattice gauge theory at finite chemical potential. *Nucl. Phys. B* **1999**, *558*, 327–346. [CrossRef]
5. Kogut, J.B.; Sinclair, D.K.; Hands, S.J.; Morrison, S.E. Two color QCD at nonzero quark number density. *Phys. Rev. D* **2001**, *64*, 094505. [CrossRef]
6. Hands, S.; Montvay, I.; Scorzato, L.; Skullerud, J. Diquark condensation in dense adjoint matter. *Eur. Phys. J. C* **2001**, *22*, 451–461. [CrossRef]
7. Muroya, S.; Nakamura, A.; Nonaka, C. Behavior of hadrons at finite density: Lattice study of color SU(2) QCD. *Phys. Lett. B* **2003**, *551*, 305–310. [CrossRef]
8. Muroya, S.; Nakamura, A.; Nonaka, C.; Takaishi, T. Lattice QCD at finite density: An Introductory review. *Prog. Theor. Phys.* **2003**, *110*, 615–668. [CrossRef]
9. Chandrasekharan, S.; Jiang, F.J. Phase-diagram of two-color lattice QCD in the chiral limit. *Phys. Rev. D* **2006**, *74*, 014506. [CrossRef]
10. Hands, S.; Kim, S.; Skullerud, J.I. Deconfinement in dense 2-color QCD. *Eur. Phys. J. C* **2006**, *48*, 193. [CrossRef]

11. Hands, S.; Sitch, P.; Skullerud, J.I. Hadron Spectrum in a Two-Colour Baryon-Rich Medium. *Phys. Lett. B* **2008**, *662*, 405–412. [CrossRef]

12. Hands, S.; Kim, S.; Skullerud, J.I. A Quarkyonic Phase in Dense Two Color Matter? *Phys. Rev. D* **2010**, *81*, 091502. [CrossRef]

13. Cotter, S.; Giudice, P.; Hands, S.; Skullerud, J.I. Towards the phase diagram of dense two-color matter. *Phys. Rev. D* **2013**, *87*, 034507. [CrossRef]

14. Hands, S.; Kim, S.; Skullerud, J.I. Non-relativistic spectrum of two-color QCD at non-zero baryon density. *Phys. Lett. B* **2012**, *711*, 199–204. [CrossRef]

15. Boz, T.; Cotter, S.; Fister, L.; Mehta, D.; Skullerud, J.I. Phase transitions and gluodynamics in 2-colour matter at high density. *Eur. Phys. J. A* **2013**, *49*, 87. [CrossRef]

16. Braguta, V.V.; Ilgenfritz, E.M.; Kotov, A.Y.; Molochkov, A.V.; Nikolaev, A.A. Study of the phase diagram of dense two-color QCD within lattice simulation. *Phys. Rev. D* **2016**, *94*, 114510. [CrossRef]

17. Puhr, M.; Buividovich, P.V. Numerical Study of Nonperturbative Corrections to the Chiral Separation Effect in Quenched Finite-Density QCD. *Phys. Rev. Lett.* **2017**, *118*, 192003. [CrossRef] [PubMed]

18. Boz, T.; Hajizadeh, O.; Maas, A.; Skullerud, J.I. Finite-density gauge correlation functions in QC2D. *Phys. Rev. D* **2019**, *99*, 074514. [CrossRef]

19. Astrakhantsev, N.Y.; Bornyakov, V.G.; Braguta, V.V.; Ilgenfritz, E.M.; Kotov, A.Y.; Nikolaev, A.A.; Rothkopf, A. Lattice study of static quark-antiquark interactions in dense quark matter. *J. High Energy Phys.* **2019**, *05*, 171. [CrossRef]

20. Iida, K.; Itou, E.; Lee, T.G. Two-colour QCD phases and the topology at low temperature and high density. *J. High Energy Phys.* **2020**, *1*, 181. [CrossRef]

21. Wilhelm, J.; Holicki, L.; Smith, D.; Wellegehausen, B.; von Smekal, L. Continuum Goldstone spectrum of two-color QCD at finite density with staggered quarks. *Phys. Rev. D* **2019**, *100*, 114507. [CrossRef]

22. Boz, T.; Giudice, P.; Hands, S.; Skullerud, J.I. Dense two-color QCD towards continuum and chiral limits. *Phys. Rev. D* **2020**, *101*, 074506. [CrossRef]

23. Buividovich, P.V.; Smith, D.; von Smekal, L. Numerical study of the chiral separation effect in two-color QCD at finite density. *Phys. Rev. D* **2021**, *104*, 014511. [CrossRef]

24. Iida, K.; Itou, E.; Lee, T.G. Relative scale setting for two-color QCD with N_f = 2 Wilson fermions. *Prog. Theor. Exp. Phys.* **2021**, *2021*, 013B05. [CrossRef]

25. Astrakhantsev, N.; Braguta, V.V.; Ilgenfritz, E.M.; Kotov, A.Y.; Nikolaev, A.A. Lattice study of thermodynamic properties of dense QC$_2$D. *Phys. Rev. D* **2020**, *102*, 074507. [CrossRef]

26. Bornyakov, V.G.; Braguta, V.V.; Nikolaev, A.A.; Rogalyov, R.N. Effects of Dense Quark Matter on Gluon Propagators in Lattice QC$_2$D. *Phys. Rev. D* **2020**, *102*, 114511. [CrossRef]

27. Buividovich, P.V.; Smith, D.; von Smekal, L. Electric conductivity in finite-density $SU(2)$ lattice gauge theory with dynamical fermions. *Phys. Rev. D* **2020**, *102*, 094510. [CrossRef]

28. Buividovich, P.V.; Smith, D.; von Smekal, L. Static magnetic susceptibility in finite-density $SU(2)$ lattice gauge theory. *Eur. Phys. J. A* **2021**, *57*, 293. [CrossRef]

29. Begun, A.; Bornyakov, V.G.; Gerasimeniuk, N.V.; Goy, V.A.; Nakamura, A.; Rogalyov, R.N.; Vovchenko, V. Quark Density in Lattice QC$_2$D at Imaginary and Real Chemical Potential. *arXiv* **2021**, arXiv:2103.07442.

30. Iida, K.; Itou, E. Velocity of Sound beyond the High-Density Relativistic Limit from Lattice Simulation of Dense Two-Color QCD. *arXiv* **2022**, arXiv:2207.01253. [CrossRef]

31. Begun, A.; Bornyakov, V.G.; Goy, V.A.; Nakamura, A.; Rogalyov, R.N. Study of two color QCD on large lattices. *Phys. Rev. D* **2022**, *105*, 114505. [CrossRef]

32. Murakami, K.; Itou, E.; Iida, K. Chemical potential (in)dependence of hadron scatterings in the hadronic phase of QCD-like theories and its applications. *arXiv* **2023**, arXiv:2309.08143. [CrossRef]

33. Braguta, V.V. Phase Diagram of Dense Two-Color QCD at Low Temperatures. *Symmetry* **2023**, *15*, 1466. [CrossRef]

34. Iida, K.; Itou, E.; Murakami, K.; Suenaga, D. Lattice study on finite density QC$_2$D towards zero temperature. *J. High Energy Phys.* **2024**, *10*, 022. [CrossRef]

35. Pauli, W. On the conservation of the Lepton charge. *Nuovo Cim.* **1957**, *6*, 204–215. [CrossRef]

36. Gürsey, F. Relation of charge independence and baryon conservation to Pauli's transformation. *Nuovo Cim.* **1958**, *7*, 411–415. [CrossRef]

37. Gasser, J.; Leutwyler, H. Chiral Perturbation Theory to One Loop. *Ann. Phys.* **1984**, *158*, 142. [CrossRef]

38. Gasser, J.; Leutwyler, H. Chiral Perturbation Theory: Expansions in the Mass of the Strange Quark. *Nucl. Phys. B* **1985**, *250*, 465–516. [CrossRef]

39. Kogut, J.B.; Stephanov, M.A.; Toublan, D. On two color QCD with baryon chemical potential. *Phys. Lett. B* **1999**, *464*, 183–191. [CrossRef]

40. Kogut, J.B.; Stephanov, M.A.; Toublan, D.; Verbaarschot, J.J.M.; Zhitnitsky, A. QCD—Like theories at finite baryon density. *Nucl. Phys. B* **2000**, *582*, 477–513. [CrossRef]

41. Murakami, K.; Suenaga, D.; Iida, K.; Itou, E. Measurement of hadron masses in 2-color finite density QCD. *PoS* **2023**, *LATTICE2022*, 154. [CrossRef]

42. Coleman, S.R.; Wess, J.; Zumino, B. Structure of phenomenological Lagrangians. 1. *Phys. Rev.* **1969**, *177*, 2239–2247. [CrossRef]

43. Callan, C.G., Jr.; Coleman, S.R.; Wess, J.; Zumino, B. Structure of phenomenological Lagrangians. 2. *Phys. Rev.* **1969**, *177*, 2247–2250. [CrossRef]

44. Suenaga, D.; Murakami, K.; Itou, E.; Iida, K. Probing the hadron mass spectrum in dense two-color QCD with the linear sigma model. *Phys. Rev. D* **2023**, *107*, 054001. [CrossRef]

45. Lenaghan, J.T.; Sannino, F.; Splittorff, K. The Superfluid and conformal phase transitions of two color QCD. *Phys. Rev. D* **2002**, *65*, 054002. [CrossRef]

46. Splittorff, K.; Toublan, D.; Verbaarschot, J.J.M. Diquark condensate in QCD with two colors at next-to-leading order. *Nucl. Phys. B* **2002**, *620*, 290–314. [CrossRef]

47. Ratti, C.; Weise, W. Thermodynamics of two-colour QCD and the Nambu Jona-Lasinio model. *Phys. Rev. D* **2004**, *70*, 054013. [CrossRef]

48. Sun, G.f.; He, L.; Zhuang, P. BEC-BCS crossover in the Nambu-Jona-Lasinio model of QCD. *Phys. Rev. D* **2007**, *75*, 096004. [CrossRef]

49. Fukushima, K.; Iida, K. Larkin-Ovchinnikov-Fulde-Ferrell state in two-color quark matter. *Phys. Rev. D* **2007**, *76*, 054004. [CrossRef]

50. Brauner, T.; Fukushima, K.; Hidaka, Y. Two-color quark matter: U(1)(A) restoration, superfluidity, and quarkyonic phase. *Phys. Rev. D* **2009**, *80*, 074035; Erratum in *Phys. Rev. D* **2010**, *81*, 119904. [CrossRef]

51. Kanazawa, T.; Wettig, T.; Yamamoto, N. Chiral Lagrangian and spectral sum rules for dense two-color QCD. *J. High Energy Phys.* **2009**, *8*, 3. [CrossRef]

52. Harada, M.; Nonaka, C.; Yamaoka, T. Masses of vector bosons in two-color dense QCD based on the hidden local symmetry. *Phys. Rev. D* **2010**, *81*, 096003. [CrossRef]

53. Andersen, J.O.; Brauner, T. Phase diagram of two-color quark matter at nonzero baryon and isospin density. *Phys. Rev. D* **2010**, *81*, 096004. [CrossRef]

54. Zhang, T.; Brauner, T.; Rischke, D.H. QCD-like theories at nonzero temperature and density. *J. High Energy Phys.* **2010**, *6*, 64. [CrossRef]

55. He, L. Nambu-Jona-Lasinio model description of weakly interacting Bose condensate and BEC-BCS crossover in dense QCD-like theories. *Phys. Rev. D* **2010**, *82*, 096003. [CrossRef]

56. Strodthoff, N.; Schaefer, B.J.; von Smekal, L. Quark-meson-diquark model for two-color QCD. *Phys. Rev. D* **2012**, *85*, 074007. [CrossRef]

57. Imai, S.; Toki, H.; Weise, W. Quark-Hadron Matter at Finite Temperature and Density in a Two-Color PNJL model. *Nucl. Phys. A* **2013**, *913*, 71–102. [CrossRef]

58. Strodthoff, N.; von Smekal, L. Polyakov-Quark-Meson-Diquark Model for two-color QCD. *Phys. Lett. B* **2014**, *731*, 350–357. [CrossRef]

59. Khan, N.; Pawlowski, J.M.; Rennecke, F.; Scherer, M.M. The Phase Diagram of QC2D from Functional Methods. *arxiv* **2015**, arXiv:1512.03673.

60. Duarte, D.C.; Allen, P.G.; Farias, R.L.S.; Manso, P.H.A.; Ramos, R.O.; Scoccola, N.N. BEC-BCS crossover in a cold and magnetized two color NJL model. *Phys. Rev. D* **2016**, *93*, 025017. [CrossRef]

61. Chao, J. Phase diagram of two-color QCD matter at finite baryon and axial isospin densities. *Chin. Phys. C* **2020**, *44*, 034108. [CrossRef]

62. Adhikari, P.; Beleznay, S.B.; Mannarelli, M. Finite Density Two Color Chiral Perturbation Theory Revisited. *Eur. Phys. J. C* **2018**, *78*, 441. [CrossRef]

63. Contant, R.; Huber, M.Q. Dense two-color QCD from Dyson-Schwinger equations. *Phys. Rev. D* **2020**, *101*, 014016. [CrossRef]

64. Suenaga, D.; Kojo, T. Gluon propagator in two-color dense QCD: Massive Yang-Mills approach at one-loop. *Phys. Rev. D* **2019**, *100*, 076017. [CrossRef]

65. Khunjua, T.G.; Klimenko, K.G.; Zhokhov, R.N. The dual properties of chiral and isospin asymmetric dense quark matter formed of two-color quarks. *J. High Energy Phys.* **2020**, *6*, 148. [CrossRef]

66. Kojo, T.; Suenaga, D. Thermal quarks and gluon propagators in two-color dense QCD. *Phys. Rev. D* **2021**, *103*, 094008. [CrossRef]

67. Suenaga, D.; Kojo, T. Delineating chiral separation effect in two-color dense QCD. *Phys. Rev. D* **2021**, *104*, 034038. [CrossRef]

68. Kojo, T.; Suenaga, D. Peaks of sound velocity in two color dense QCD: Quark saturation effects and semishort range correlations. *Phys. Rev. D* **2022**, *105*, 076001. [CrossRef]

69. Khunjua, T.G.; Klimenko, K.G.; Zhokhov, R.N. Influence of chiral chemical potential μ_5 on phase structure of the two-color quark matter. *Phys. Rev. D* **2022**, *106*, 045008. [CrossRef]

70. Kawaguchi, M.; Suenaga, D. Fate of the topological susceptibility in two-color dense QCD. *J. High Energy Phys.* **2023**, *08*, 189. [CrossRef]

71. Suenaga, D.; Murakami, K.; Itou, E.; Iida, K. Mass spectrum of spin-one hadrons in dense two-color QCD: Novel predictions by extended linear sigma model. *Phys. Rev. D* **2024**, *109*, 074031. [CrossRef]

72. Kawaguchi, M.; Suenaga, D. Sound velocity peak induced by the chiral partner in dense two-color QCD. *Phys. Rev. D* **2024**, *109*, 096034. [CrossRef]

73. Acharyya, N.; Aich, P.; Bandyopadhyay, A.; Vaidya, S. Matrix model of two-color one-flavor QCD: The ultrastrong coupling regime. *Phys. Rev. D* **2024**, *110*, 054016. [CrossRef]

74. Khunjua, T.G.; Klimenko, K.G.; Zhokhov, R.N. Dual symmetries of dense three and two-color QCD and some QCD-like NJL models. *arXiv* **2024**, arXiv:2403.00444.

75. Cheng, T.; Li, L. *Gauge Theory of Elementary Particle Physics*; Oxford University Press: Oxford, UK, 1995.

76. Bando, M.; Kugo, T.; Yamawaki, K. Nonlinear Realization and Hidden Local Symmetries. *Phys. Rept.* **1988**, *164*, 217–314. [CrossRef]

77. Son, D.T.; Stephanov, M.A. QCD at finite isospin density: From pion to quark - anti-quark condensation. *Phys. Atom. Nucl.* **2001**, *64*, 834–842. [CrossRef]

78. Harada, M.; Yamawaki, K. Hidden local symmetry at loop: A New perspective of composite gauge boson and chiral phase transition. *Phys. Rept.* **2003**, *381*, 1–233. [CrossRef]

79. Murakami, K.; Suenaga, D.; Itou, E.; Iida, K. in preparation.

80. Witten, E. Baryons in the 1/n Expansion. *Nucl. Phys. B* **1979**, *160*, 57–115. [CrossRef]

81. Fejos, G.; Hosaka, A. Thermal properties and evolution of the $U_A(1)$ factor for 2+1 flavors. *Phys. Rev. D* **2016**, *94*, 036005. [CrossRef]

82. Fejős, G.; Hosaka, A. Mesonic and nucleon fluctuation effects at finite baryon density. *Phys. Rev. D* **2017**, *95*, 116011. [CrossRef]

83. Lombardo, M.P. Topological Aspects of Dense Matter: Lattice Studies. *Universe* **2021**, *7*, 336. [CrossRef]

84. Fujikawa, K. Path Integral Measure for Gauge Invariant Fermion Theories. *Phys. Rev. Lett.* **1979**, *42*, 1195–1198. [CrossRef]

85. Parganlija, D.; Giacosa, F.; Rischke, D.H. Vacuum Properties of Mesons in a Linear Sigma Model with Vector Mesons and Global Chiral Invariance. *Phys. Rev. D* **2010**, *82*, 054024. [CrossRef]

86. Parganlija, D.; Kovacs, P.; Wolf, G.; Giacosa, F.; Rischke, D.H. Meson vacuum phenomenology in a three-flavor linear sigma model with (axial-)vector mesons. *Phys. Rev. D* **2013**, *87*, 014011. [CrossRef]

87. Son, D.T.; Stephanov, M.A. QCD at finite isospin density. *Phys. Rev. Lett.* **2001**, *86*, 592–595. [CrossRef] [PubMed]

88. Splittorff, K.; Son, D.T.; Stephanov, M.A. QCD—Like theories at finite baryon and isospin density. *Phys. Rev. D* **2001**, *64*, 016003. [CrossRef]

89. Lu, Z.Y.; Xia, C.J.; Ruggieri, M. Thermodynamics and susceptibilities of isospin imbalanced QCD matter. *Eur. Phys. J. C* **2020**, *80*, 46. [CrossRef]

90. Gómez Nicola, A.; Vioque-Rodríguez, A. Effective Lagrangian at nonzero isospin chemical potential. *Phys. Rev. D* **2022**, *106*, 114017. [CrossRef]

91. Brandt, B.B.; Cuteri, F.; Endrodi, G. Equation of state and speed of sound of isospin-asymmetric QCD on the lattice. *J. High Energy Phys.* **2023**, *7*, 55. [CrossRef]

92. Abbott, R.; Detmold, W.; Romero-López, F.; Davoudi, Z.; Illa, M.; Parreño, A.; Perry, R.J.; Shanahan, P.E.; Wagman, M.L. Lattice quantum chromodynamics at large isospin density. *Phys. Rev. D* **2023**, *108*, 114506. [CrossRef]

93. Abbott, R.; Detmold, W.; Illa, M.; Parreño, A.; Perry, R.J.; Romero-López, F.; Shanahan, P.E.; Wagman, M.L. QCD constraints on isospin-dense matter and the nuclear equation of state. *arXiv* **2024**, arXiv:2406.09273. [CrossRef]

94. Komoltsev, O.; Kurkela, A. How Perturbative QCD Constrains the Equation of State at Neutron-Star Densities. *Phys. Rev. Lett.* **2022**, *128*, 202701. [CrossRef] [PubMed]

95. Koehn, H.; Rose, H.; Pang, P.T.H.; Somasundaram, R.; Reed, B.T. From existing and new nuclear and astrophysical constraints to stringent limits on the equation of state of neutron-rich dense matter. *arXiv* **2024**, arXiv:2402.04172.

96. Hochberg, Y.; Kuflik, E.; Murayama, H.; Volansky, T.; Wacker, J.G. Model for Thermal Relic Dark Matter of Strongly Interacting Massive Particles. *Phys. Rev. Lett.* **2015**, *115*, 021301. [CrossRef]

97. Detmold, W.; McCullough, M.; Pochinsky, A. Dark nuclei. II. Nuclear spectroscopy in two-color QCD. *Phys. Rev. D* **2014**, *90*, 114506. [CrossRef]

98. Hochberg, Y.; Kuflik, E.; Murayama, H. SIMP Spectroscopy. *J. High Energy Phys.* **2016**, *5*, 90. [CrossRef]

99. Kamada, A.; Kobayashi, S.; Kuwahara, T. Perturbative unitarity of strongly interacting massive particle models. *J. High Energy Phys.* **2023**, *2*, 217. [CrossRef]

100. Kulkarni, S.; Maas, A.; Mee, S.; Nikolic, M.; Pradler, J.; Zierler, F. Low-energy effective description of dark $Sp(4)$ theories. *SciPost Phys.* **2023**, *14*, 44. [CrossRef]

101. Chu, X.; Nikolic, M.; Pradler, J. Even SIMP miracles are possible. *Phys. Rev. Lett.* **2024**, *133*, 2. [CrossRef]

102. Dengler, Y.; Maas, A.; Zierler, F. Scattering of dark pions in Sp(4) gauge theory. *Phys. Rev. D* **2024**, *110*, 054513. [CrossRef]

103. Manohar, A.; Wise, M.; Ericson, T.; Landshoff, P. *Heavy Quark Physics*; Cambridge Monographs on Particle Physics, Nuclear Physics and Cosmology, Cambridge University Press: Cambridge, UK, 2000.

104. Harada, M.; Liu, Y.R.; Oka, M.; Suzuki, K. Chiral effective theory of diquarks and the $U_A(1)$ anomaly. *Phys. Rev. D* **2020**, *101*, 054038. [CrossRef]

105. Suenaga, D.; Oka, M. Axial anomaly effect on the chiral-partner structure of diquarks at high temperature. *Phys. Rev. D* **2023**, *108*, 014030. [CrossRef]

106. Suenaga, D.; Oka, M. Fate of Σ_c, Ξ_c' and Ω_c baryons at high temperature with chiral restoration. *arXiv* **2024**, arXiv:2411.12172.

107. Hess, M.; Karsch, F.; Laermann, E.; Wetzorke, I. Diquark masses from lattice QCD. *Phys. Rev. D* **1998**, *58*, 111502. [CrossRef]

108. Alexandrou, C.; de Forcrand, P.; Lucini, B. Evidence for diquarks in lattice QCD. *Phys. Rev. Lett.* **2006**, *97*, 222002. [CrossRef] [PubMed]

109. Babich, R.; Garron, N.; Hoelbling, C.; Howard, J.; Lellouch, L.; Rebbi, C. Diquark correlations in baryons on the lattice with overlap quarks. *Phys. Rev. D* **2007**, *76*, 074021. [CrossRef]

110. Bi, Y.; Cai, H.; Chen, Y.; Gong, M.; Liu, Z.; Qiao, H.X.; Yang, Y.B. Diquark mass differences from unquenched lattice QCD. *Chin. Phys. C* **2016**, *40*, 073106. [CrossRef]

111. Francis, A.; de Forcrand, P.; Lewis, R.; Maltman, K. Diquark properties from full QCD lattice simulations. *J. High Energy Phys.* **2022**, *5*, 62. [CrossRef]

112. Watanabe, K. Quark-diquark potential and diquark mass from lattice QCD. *Phys. Rev. D* **2022**, *105*, 074510. [CrossRef]